

JCU ePrints

This file is part of the following reference:

Rich, Benjamin H. (2005) *Microstructural insights into the tectonic history of the southeastern New England Appalachians; porphyroblast-matrix structural analysis and insitu geochronology of rocks from the Merrimack Terrane, Connecticut and the Narragansett Basin, Rhode Island*. PhD thesis, James Cook University.

Access to this file is available from:

<http://eprints.jcu.edu.au/2084>

**Chapter 1. Permian bulk shortening in the Narragansett
Basin of southeastern New England, USA.**

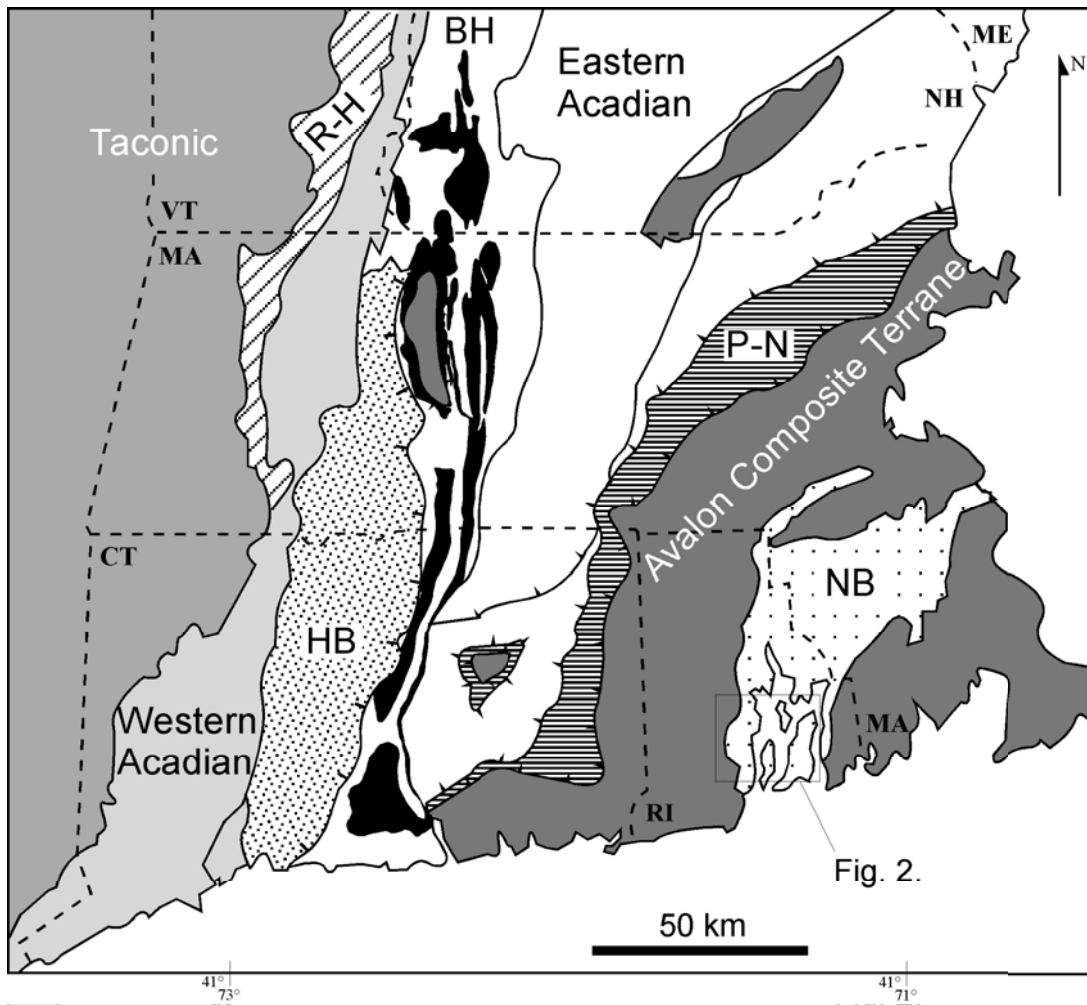


Figure 1.

The location of the area shown in Figure 3 within a regional geological map of southern New England showing the major metamorphic realms as presented by Armstrong, Tracy and Hames (1992). Also shown are the major sedimentary basins HB- Hartford Basin (Mesozoic) and the NB- Narragansett Basin (Pennsylvanian), the Middle Proterozoic Rowe Hawley terrane (R-H), the Late Proterozoic to Early Palaeozoic Putnam Nashoba terrane (P-N) and the Late Ordovician Bronson Hill magmatic arc. Regional Alleghanian metamorphism has been documented broadly within the Avalon Composite Terrane (Wintsch and Sutter, 1986). VT- Vermont, MA- Massachusetts, CT- Connecticut, ME- Maine, NH- New Hampshire, RI- Rhode Island.

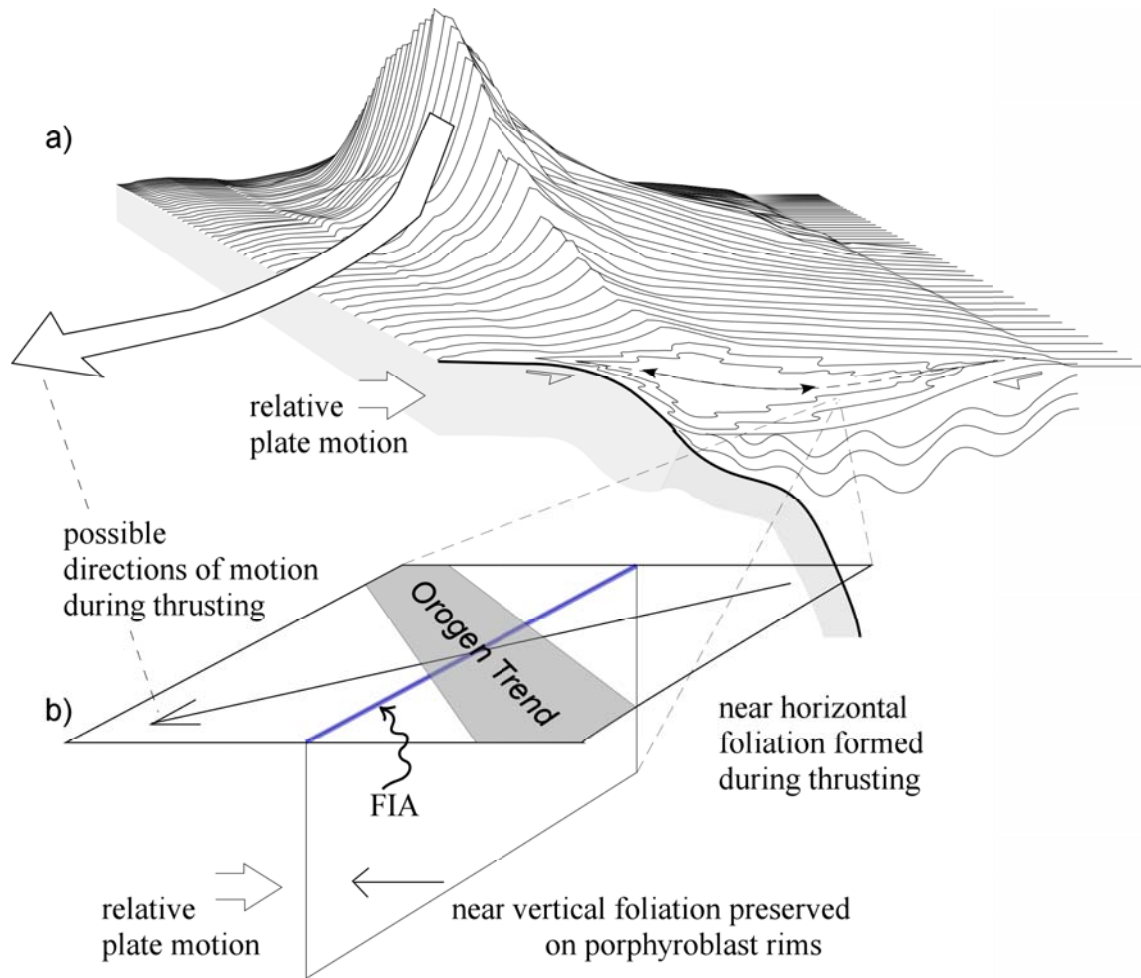


Figure 2.

a) Schematic diagram showing two colliding plates. Thrusting can occur at high angles to the topographic high created by the orogen. b) Sketch shows how the FIA trend, if generated by the intersection of the sub-vertical and sub-horizontal planes as shown, is independent of the orientation of the direction of thrusting on the horizontal foliation and can form perpendicular to the relative direction of bulk compression.

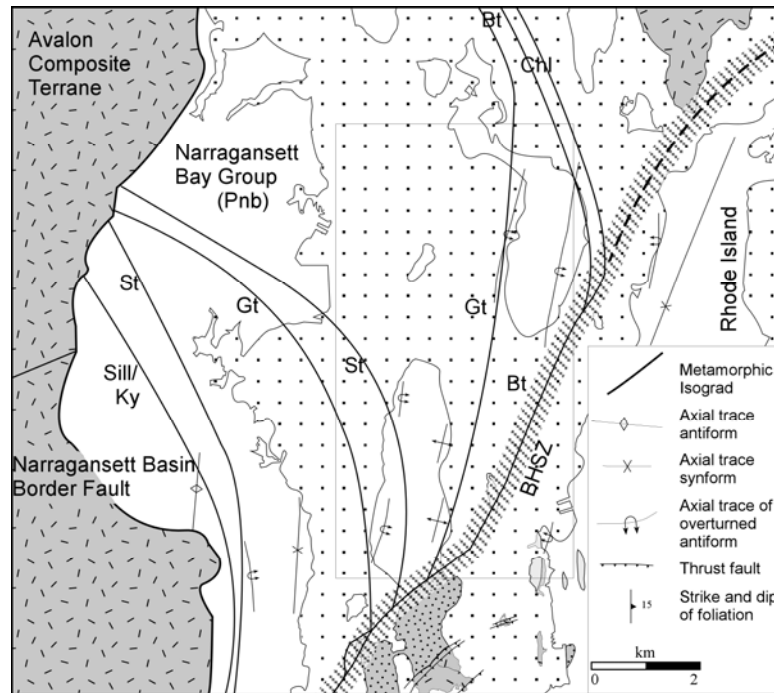


Figure 3a.

Map of a portion of Rhode Island showing the fault controlled boundaries between the Avalon Composite Terrane and the Rhode Island Formation metasediments (Pnb) of the Narragansett Basin. Isograds highlight the marked increase in metamorphic grade towards the southwest corner of the basin (modified after Hermes, O. D., Gromet, L. P. & Murray, D. P. 1994). The location of the area shown in Figure 3b is outlined with a box.

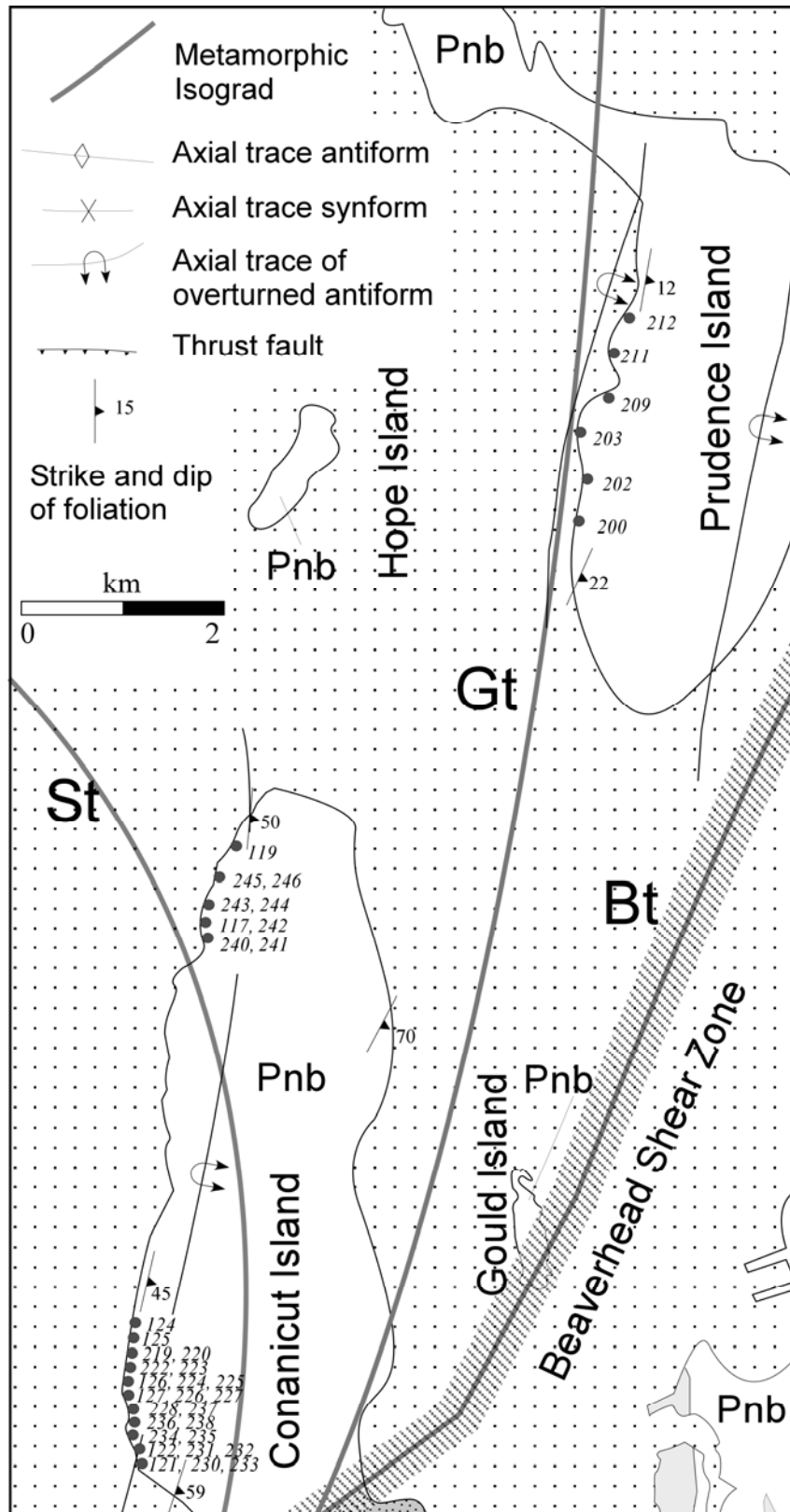


Figure 3b.

Shows the approximate localities for oriented rock samples identified by the sample numbers used in this study.

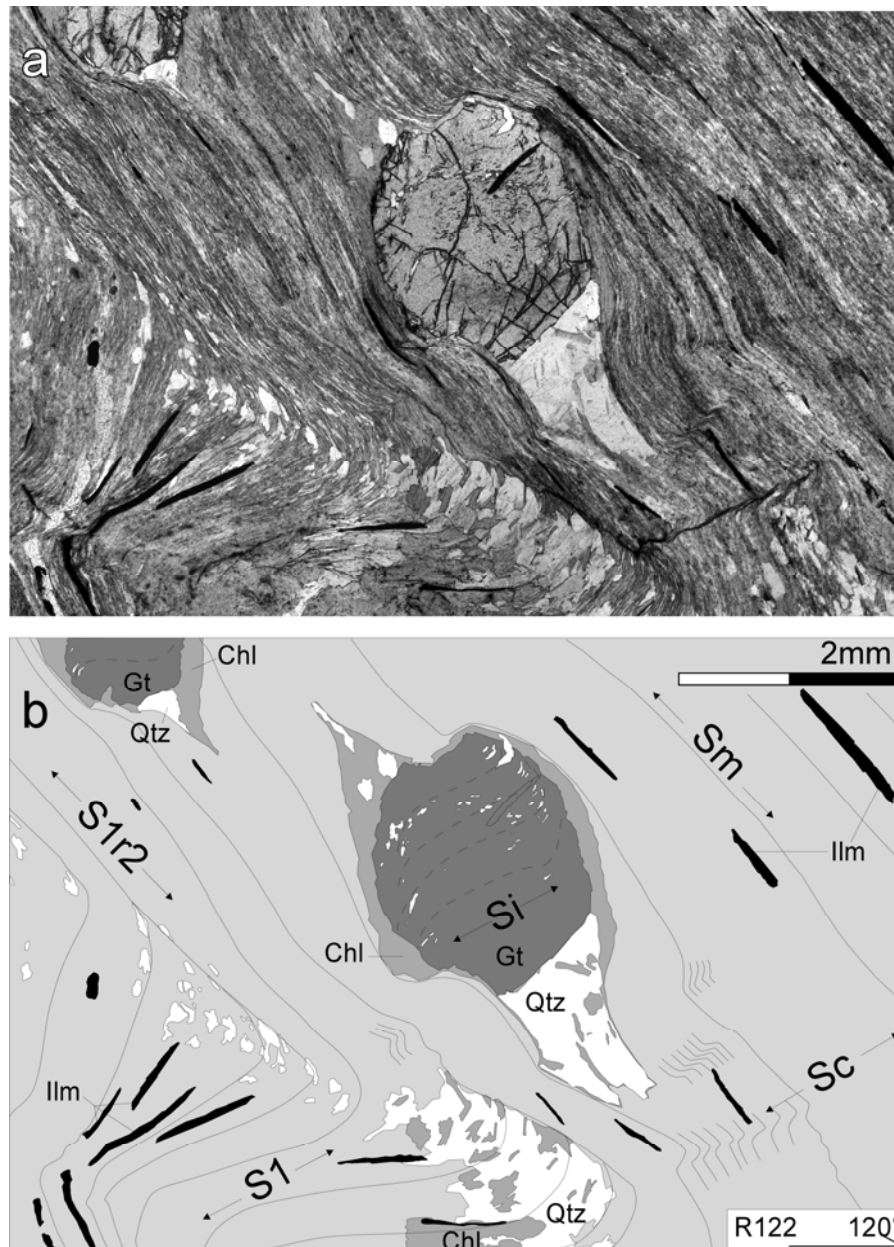


Figure 4.

(a) Photomicrograph and (b) line diagram of a vertical thin section of sample R122 from the western shore of Prudence Island (single barbed arrow indicates way up and strike at 120°). Plane polarised light. That shows simple sigmoidal ($>90^\circ$ curvature) shaped inclusion trails within a garnet porphyroblast. The internal foliation (S_i) is truncated by the external foliation. The matrix has a well developed foliation (S_m) defined by preferential alignment of muscovite and quartz plus graphite. S_1 , a foliation which predates S_m , is being reactivated and is labelled S_{1r2} . Crenulations, S_c , are defined by reoriented muscovite and quartz.

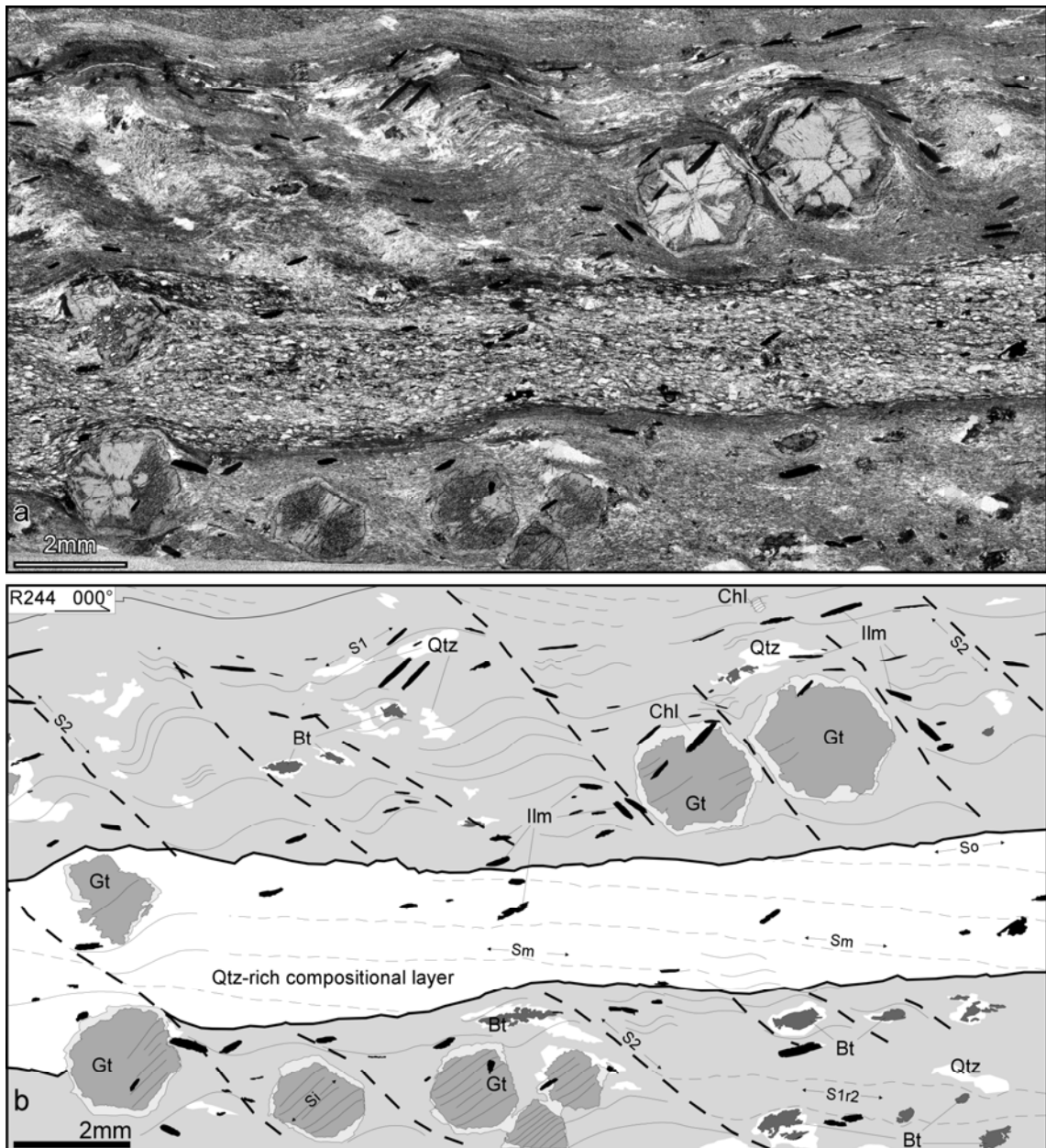


Figure 5.

(a) Photomicrograph of a vertical thin section (single barbed arrow indicates way up and strike at 000°) of sample R244 from the western shore of Conanicut Island and accompanying line diagram (b) showing a heterogeneous sub-vertical foliation S_2 overprinting a sub-horizontal foliation S_1 . Away from the porphyroblasts, S_1 is reactivated during D_2 , which decrenulates S_2 and forms S_{1r2} . The included foliation trace S_i , is continuous with the matrix. The penetrative matrix fabric (S_m) lies at a low angle to relict bedding (S_0) defined by a compositional change from muscovite-rich to quartz-rich. Plane polarised light.

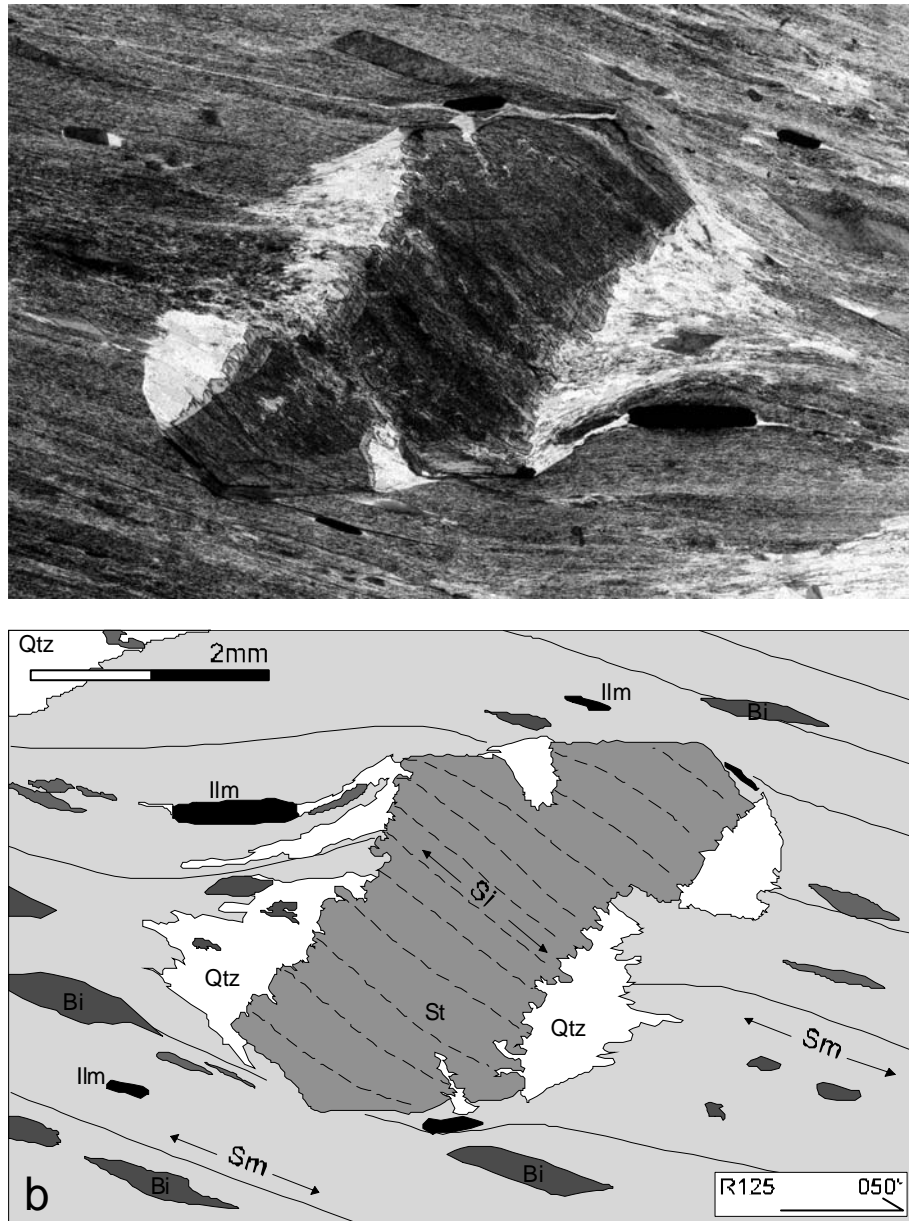


Figure 6.

(a) Photomicrograph of a vertical thin section of sample R125 (single barbed arrow indicates way up and strike at 050°) and (b) line diagram of staurolite porphyroblast with inclusion trails that are continuous with the matrix foliation labelled S_m. The matrix consists of preferentially aligned of muscovite (S_m) and graphite. Plane polarised light.

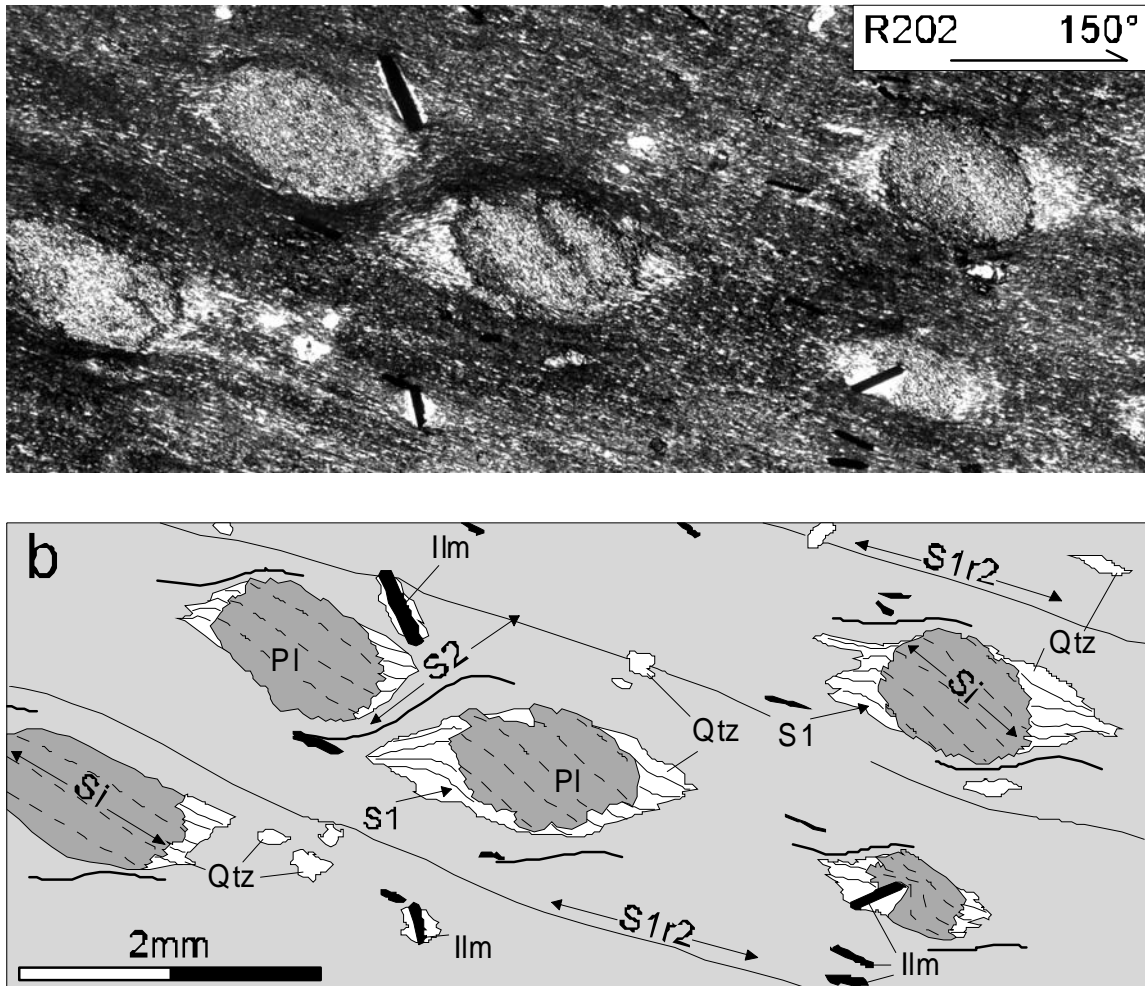


Figure 7.

(a) Photomicrograph of vertical thin section of sample R202 (single barbed arrow indicates way up and strike at 150°) and (b) line diagram of plagioclase porphyroblasts preserving a relict foliation (S_1) as inclusion trails (S_i). The dominant foliation is defined by aligned muscovite and elongate quartz grains plus graphite. Polarised light.

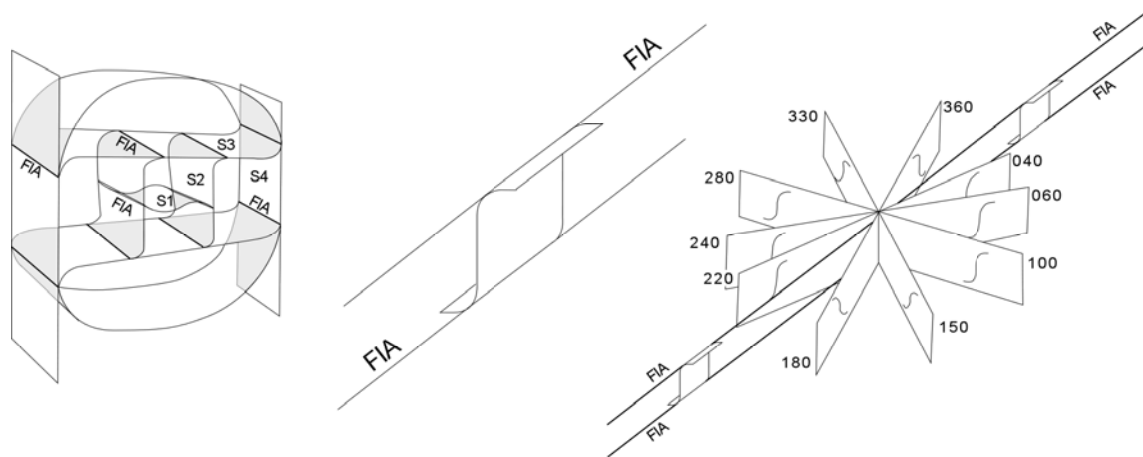


Figure 8.

(a) Diagrammatic representation of a simple sigmoidal inclusion trail showing Foliation Inflexion Axis. (b) Schematic diagram showing how the intersection of successive subvertical and subhorizontal foliations defines the foliation intersection axis or FIA, (c) The asymmetry switch method for determining FIAs (after Bell, T. H., Forde, A. & Wang, J. 1995).

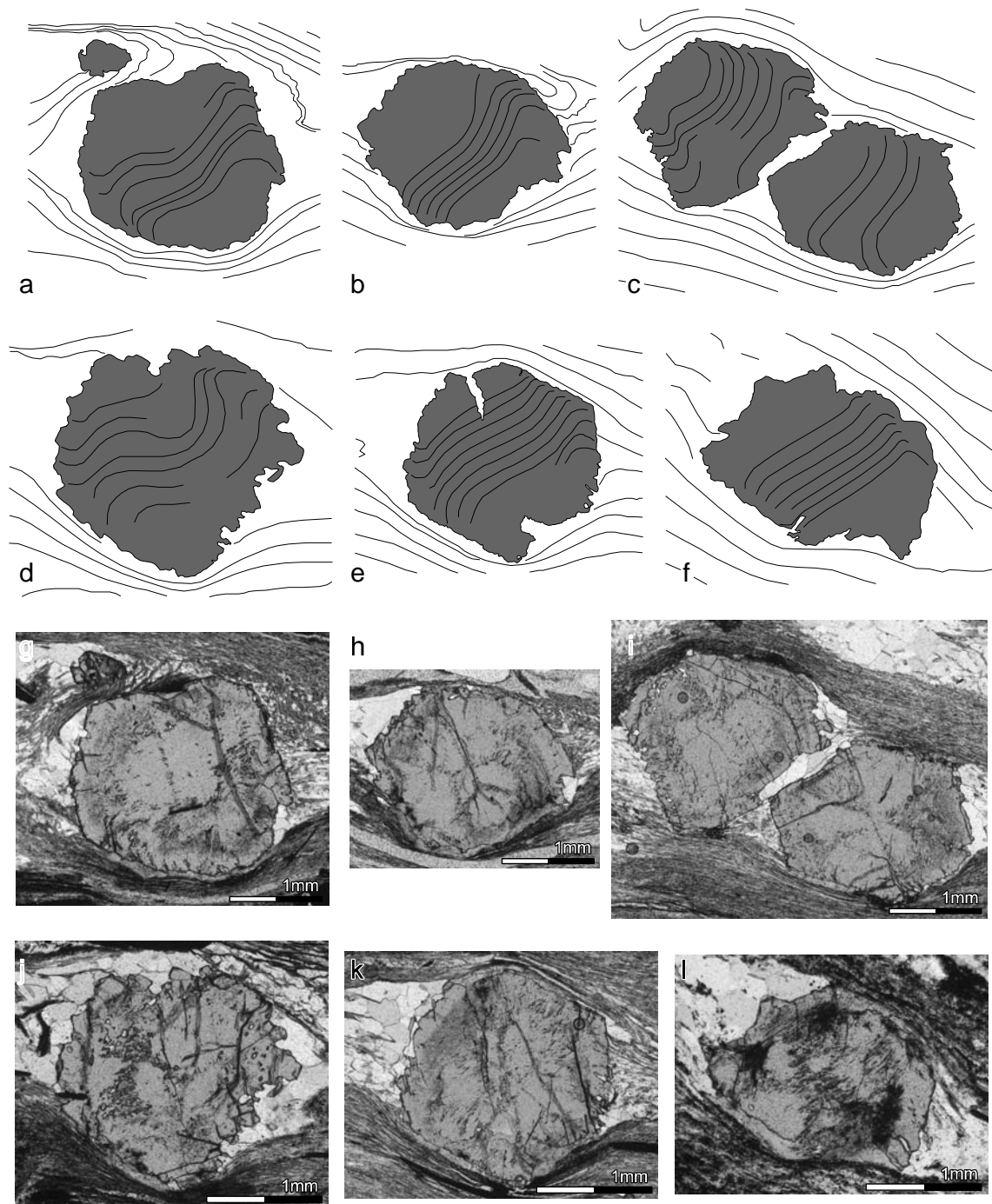


Figure 9.

Line diagrams, (a-f), and photomicrographs, (g-l), of garnet porphyroblasts from a vertical thin section striking at 40° (to the right of the page) from sample R234. The line diagrams highlight anticlockwise inclusion trail asymmetry preserved within the cores of the garnet porphyroblasts. A flip to clockwise asymmetry, in the rim of the porphyroblasts, is shown at varying degrees of preservation. Photomicrographs taken in plane polarised light.

Sample	Sm		Garnet		St	Plag	Bt
	Dip	Dip Dir.	Core	Rim			
Conanicut							
R117	39	95	75				
R119	45	103	65				
R121	28	103	15				
R122	53	85	25				
R124	19	115			40		X
R125	22	105	20	55	30		X
R126	31	111	15	80	20		X
R127	31	110		65	50		
R219	31	105	73				X
R220	26	103	18		18		X
R222	29	82	68				
R223	26	96	23		33		X
R224	22	96	63				
R225	33	89	18		18		X
R226	39	108	13	78	28		X
R227	24	103	73				X
R228	35	97			13		X
R230	40	84	13				
R231	59	93	78				
R232	59	112	18				
R233	47	103	13				
R234	28	100	8	83			
R235	44	87	13	78			
R236	48	83	18				
R237	55	83	18				
R238	23	99	18	88	18		X
R240	29	86	63			73	
R241	23	81	68			68	
R242	34	79	73				
R243	34	71		78		78	
R244	26	74	63			73	
R245	39	70				63	
R246	29	83				68	
Prudence							
R200	18	90				83	
R202	18	78				93	
R203	12	55				58	
R209	17	60				63	
R211	11	58				63	
R212	10	33				58	

Table 1.

Structural data for samples from Conanicut and Prudence islands. All samples are taken from the Rhode Island Formation. FIA data separated as staurolite (St), plagioclase (Plag) and garnet (Gt) core and rim. All orientations are relative to true north. The presence of biotite (Bt) porphyroblasts are noted with an X.

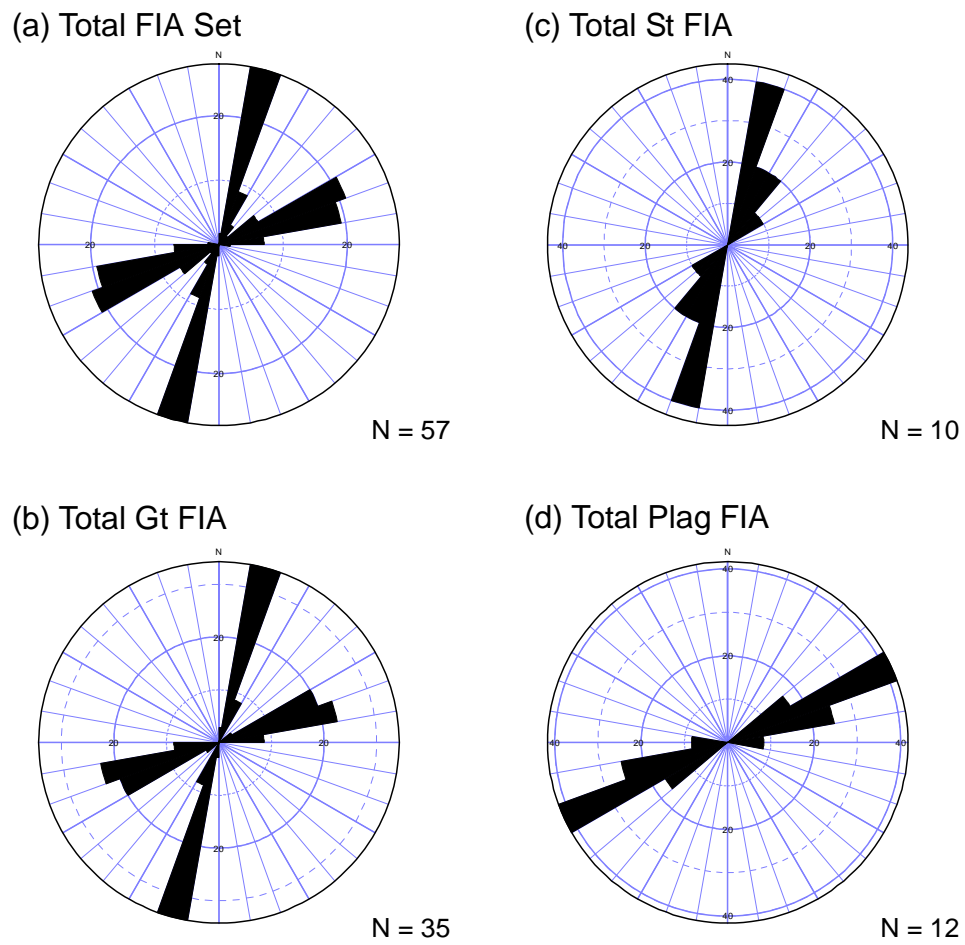


Figure 10.

(a) True area rose plot of the total FIAs for the central zone of the Narragansett Basin. For comparison, true area rose plots of FIA data for different porphyroblastic minerals (b) garnet, (c) staurolite and (d) plagioclase from the same area as (a).

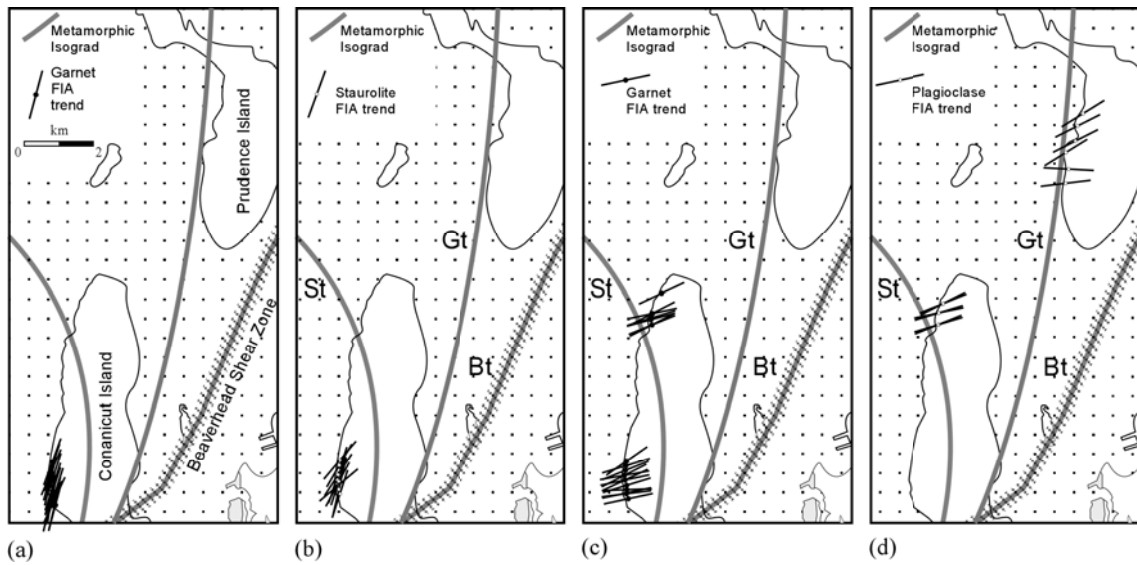


Figure 11.

FIA trends for successive FIA sets in the Narragansett Basin area. (a) Map of FIA set 1 garnet trends. (b) Map of FIA set 1 staurolite trends. (c) Map of FIA set 2 garnet trends. (d) Map of FIA set 2 plagioclase trends.

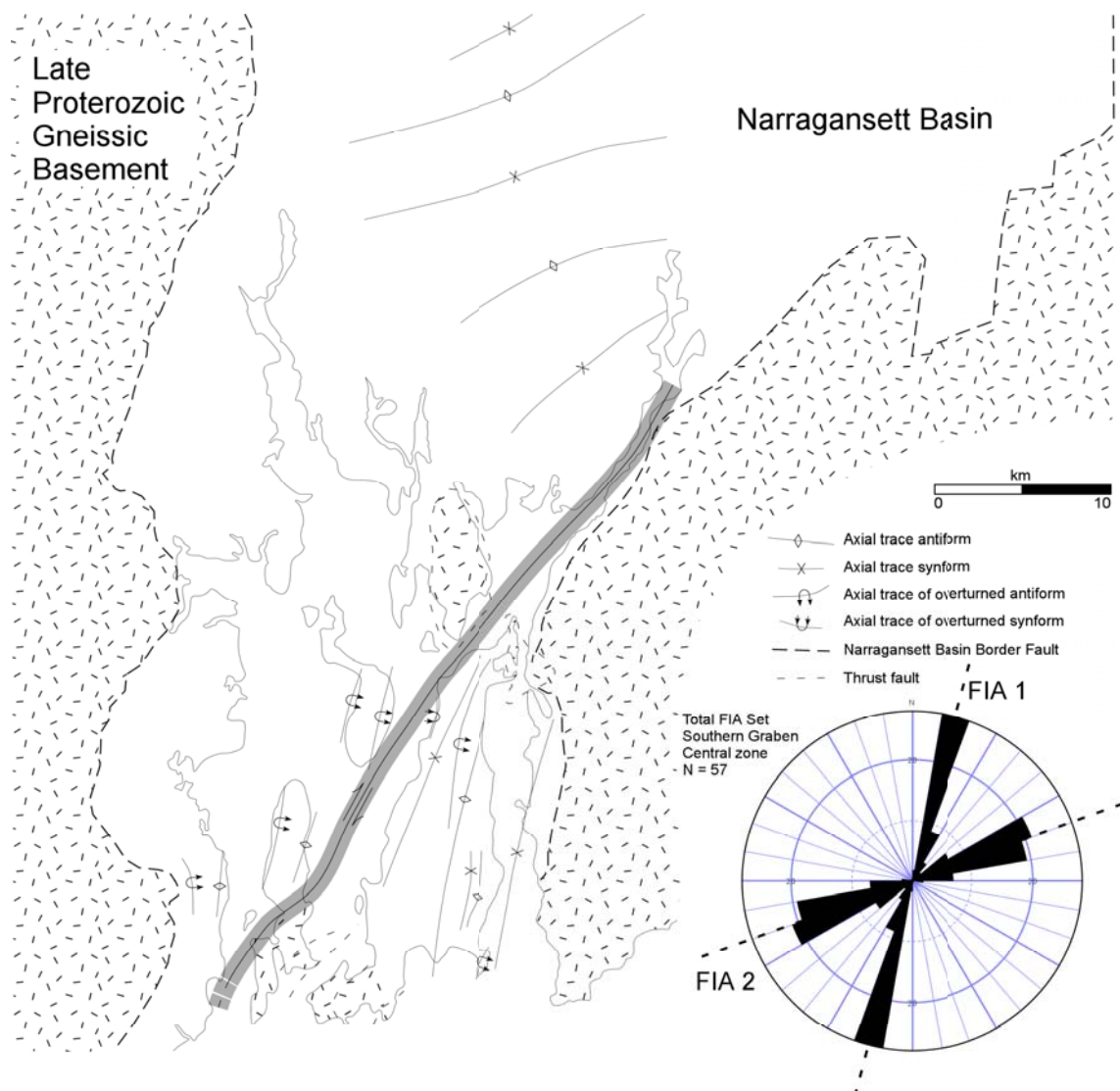


Figure 12.

Simplified geologic map of central southern Rhode Island (after Hermes, O. D., Gromet, L. P. & Murray, D. P. 1994) and true area rose plot of the total FIAs for the central zone of the southern Narragansett Basin.

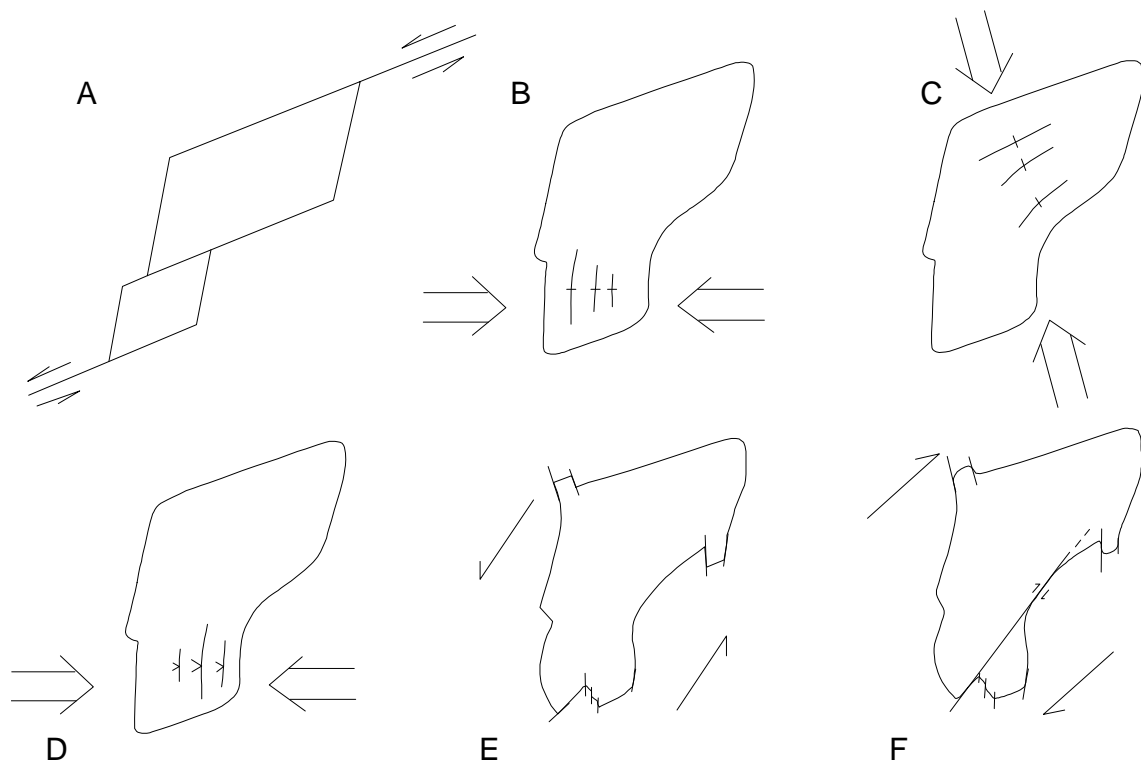


Figure 13.

Model for Narragansett Basin formation and deformation as a response to changes in motion along and within a mega shear zone between an Avalon microcontinent, the European-North American plate and the African plate. Figures modified from Mosher (1983). A, Late Palaeozoic sinistral movement resulted in the formation of pull apart basins; B, East-west compression [F_{1a} , FIA set 1] related to dextral motion forcing closure of the basin; C, North-south directed compression [F_1 folds northern graben, FIA set 2]; D, East-west compression [F_2]; E, Late-stage Alleghanian sinistral shearing; F, Subsequent dextral motion.

**Chapter 2. On shear sense using cleavages that
develop via crenulations.**

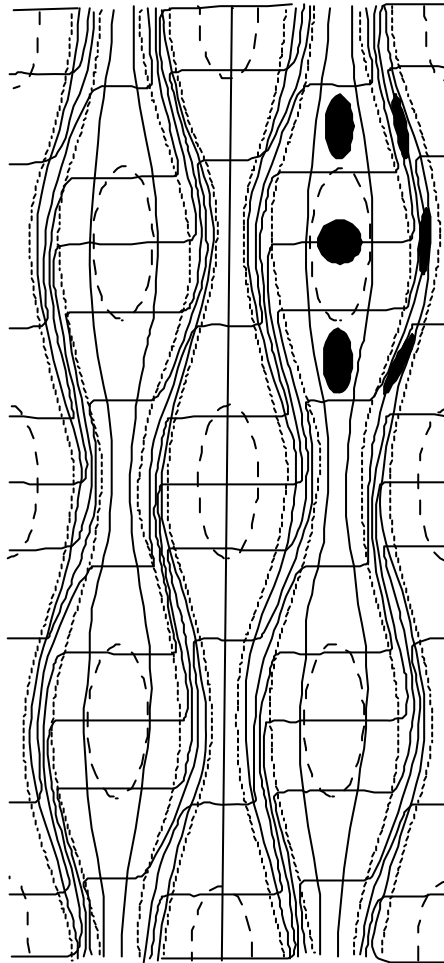


Figure 1. Strain diagram showing the conceptual distribution of strain associated with non-coaxial progressive bulk inhomogeneous shortening. Zones described by dashed lines take up no strain. Zones between dashed and dotted lines take up predominantly coaxial strain. The areas between dotted lines take up non-coaxial shearing and shortening. The anastomosing strain field lines are analogous with foliations. The conceptual orientations of local strain ellipses within these different zones are displayed as small black ellipses. This model, presented in Bell (1981), is called progressive bulk inhomogeneous shortening (PBIS).

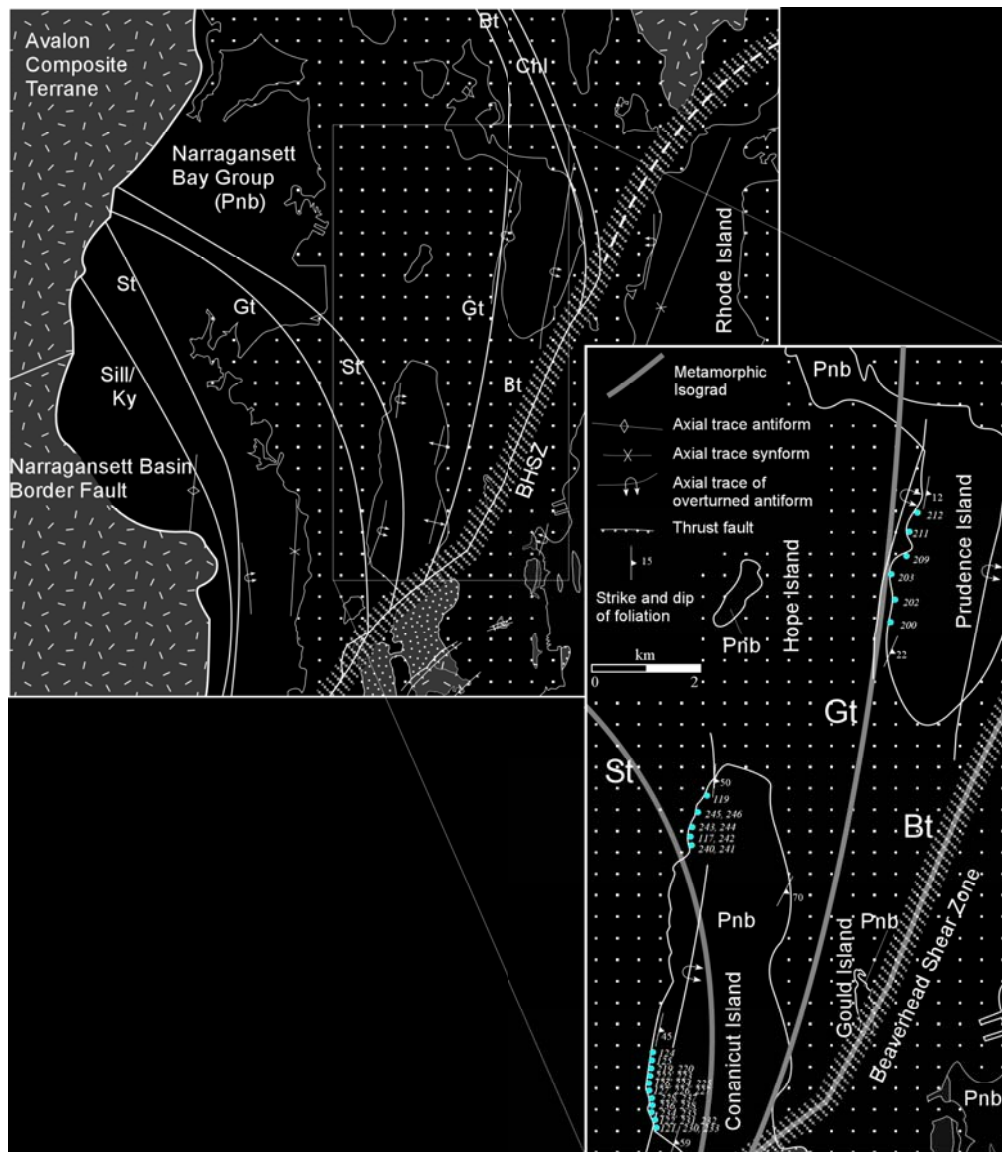


Figure 2. Map of a portion of Rhode Island showing the fault controlled boundaries between the Avalon Composite Terrane and the Rhode Island Formation metasediments (Pnb) of the Narragansett Basin. Isograds highlight the marked increase in metamorphic grade towards the southwest corner of the basin (modified after Hermes, O. D., Gromet, L. P. & Murray, D. P. 1994). The inset shows the approximate localities for oriented rock samples used in this study.

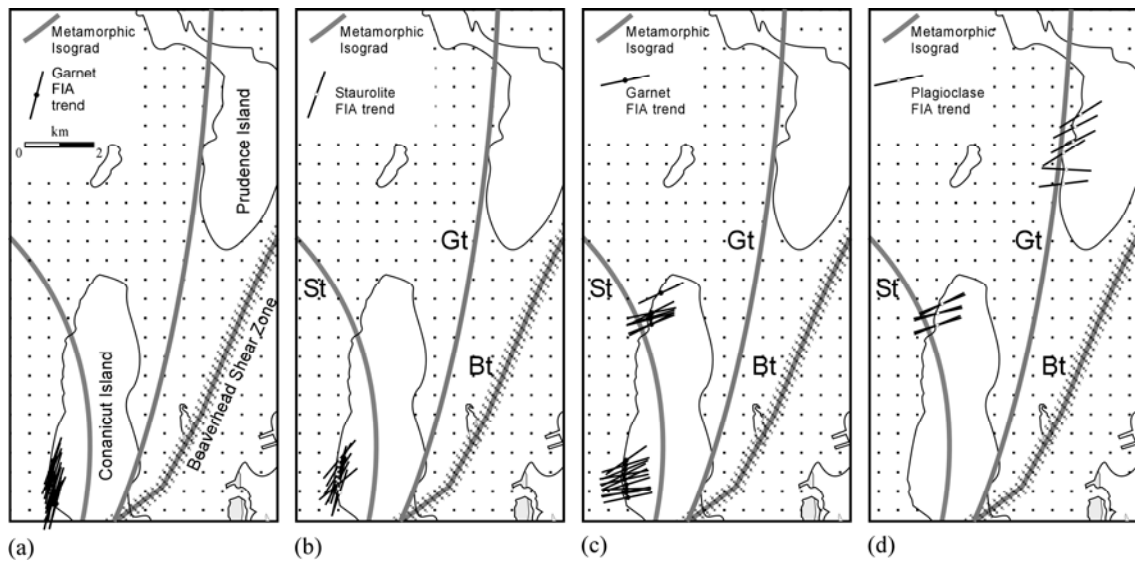


Figure 3. FIA trends for successive FIA sets in the Narragansett Basin area. (a) Map of FIA set 1 garnet trends. (b) Map of FIA set 1 staurolite trends. (c) Map of FIA set 2 garnet trends. (d) Map of FIA set 2 plagioclase trends.

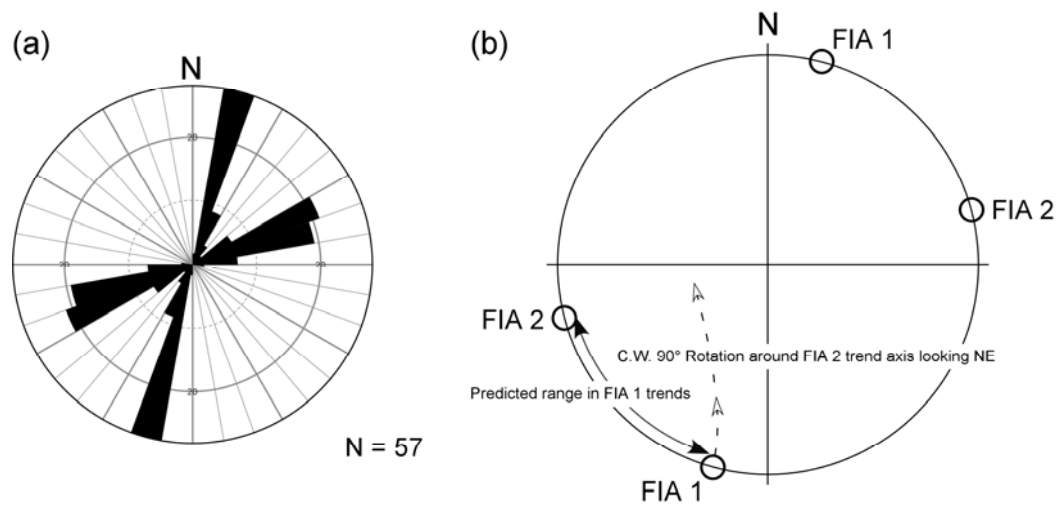
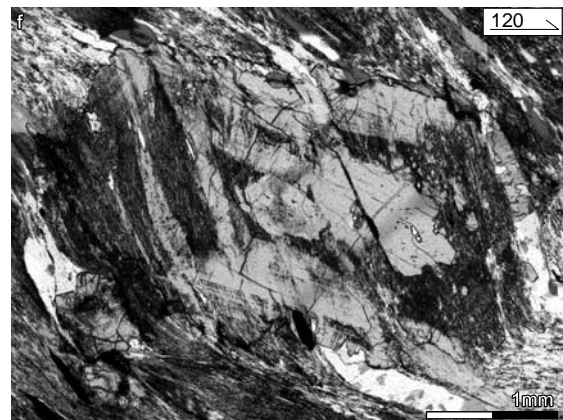
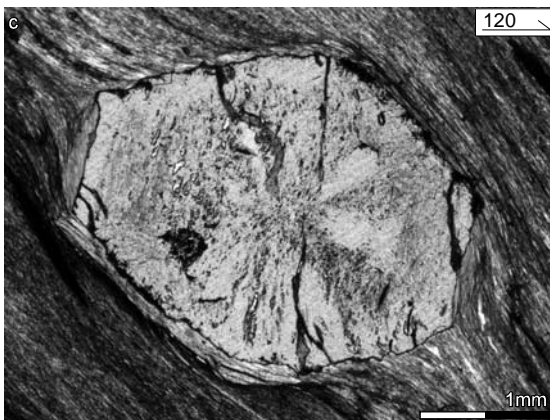
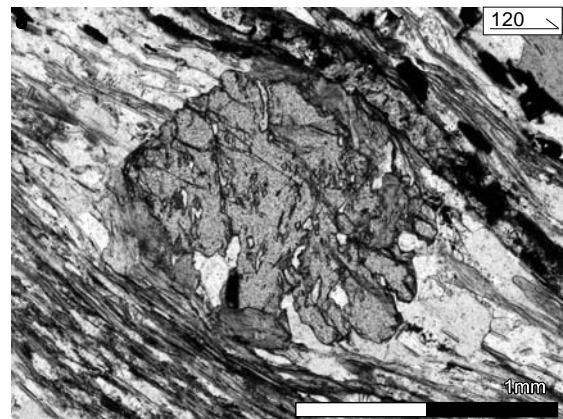
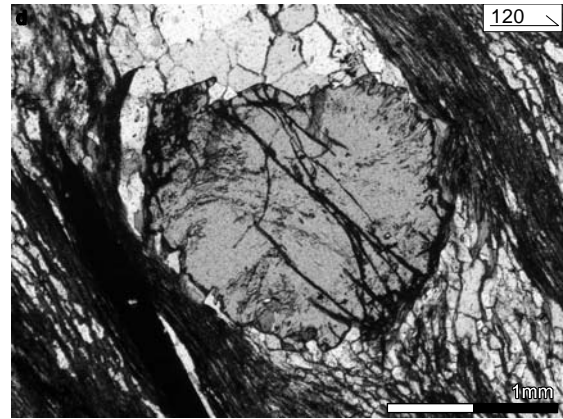
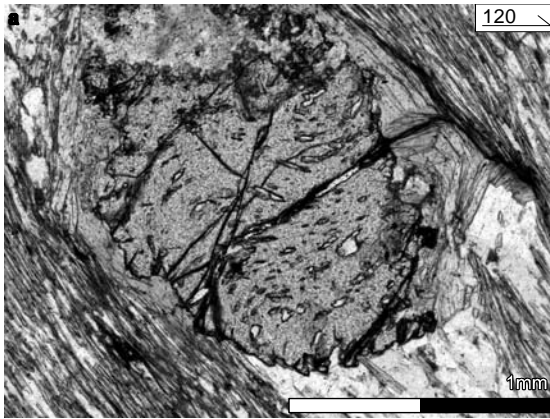


Figure 4. (a) True area rose plot of the total FIAs measured for the central zone of the Narragansett Basin. (b) Stereonet projection showing the effect of a 90° CW rotation around the mean trend of FIA set 2 on FIA set 1. A 67° resultant range in the trend of FIA 1 is predicted.

Table 1. FIA and asymmetry measurements for samples from Conanicut and Prudence islands separated as FIA sets 1 and 2. All samples are taken from the Rhode Island Formation. Mineral phase noted with sample number. All orientations are relative to true north.

SampleNo.	FIA orientation(relative to true north)		Inclusion trail asymmetry	
	Set 1	Set 2	Set 1	Set 2
R117g		075		acw(NNW)
R119g		065		acw(NNW)
R121g	015		acw(WNW)	
R122g	025		acw(WNW)	
R124st	040		acw(NW)	
R125g	020		acw(WNW)	
R125g		055		acw(NW)
R125st	030		acw(WNW)	
R126g	015		acw(WNW)	
R126g		080		acw(NNW)
R126st	020		acw(WNW)	
R127g	050	065	acw(NW)	acw(NNW)
R127st				
R219g		073		acw(NNW)
R220g	018		acw(WNW)	
R220st	018		acw(WNW)	
R222g		068		acw(NNW)
R223g	023		acw(WNW)	
R223st	033		acw(WNW)	
R224g		063		acw(NNW)
R225g	018		acw(WNW)	
R225st	018		acw(WNW)	
R226g	013		acw(WNW)	
R226g		078		acw(NNW)
R226st	028		acw(WNW)	
R227g		073		acw(NNW)
R228st	013		acw(WNW)	
R230g	013		acw(WNW)	
R231g		078		acw(NNW)
R232g	018		acw(WNW)	
R233g	013		acw(WNW)	
R234g	08		acw(WNW)	
R234g		083		acw(NNW)
R235g	013		acw(WNW)	
R235g		078		acw(NNW)
R236g	018		acw(WNW)	
R237g	018		acw(WNW)	
R238g	018		acw(WNW)	
R238g		088		acw(NNW)
R238st	018		acw(WNW)	
R240g		063		acw(NNW)
R240pl		073		acw(NNW)
R241g		068		acw(NNW)
R241pl		068		acw(NNW)
R242g		073		acw(NNW)
R243g		078		acw(NNW)
R243pl		078		acw(NNW)
R244g		063		acw(NNW)
R244pl		073		acw(NNW)
R245pl		063		acw(NNW)
R246pl		068		acw(NNW)
R200pl		083		acw(NNW)
R202pl		093		acw(NNW)
R203pl		058		acw(NW)
R209pl		063		acw(NNW)
R211pl		063		acw(NNW)
R212pl		058		acw(NW)

Figure 5. Photomicrographs from vertical thin sections orientated at N120°E (approximately perpendicular to the trend of FIA set 1). All porphyroblasts display inclusion trails with anticlockwise asymmetries. (a) Sample R233, garnet porphyroblast with chlorite alteration halo and quartz strain shadow. (b) Sample R122, garnet porphyroblast with chlorite alteration of muscovite dominated matrix adjacent to rim and quartz strain shadow. (c) Sample R237, garnet porphyroblast in muscovite dominated matrix. (d) Sample R236, garnet porphyroblast with quartz strain shadow in quartz-muscovite matrix. Large ilmenite lathe aligned with matrix in bottom-left corner. (e) Sample R230, garnet porphyroblast with chlorite altered rim within quartz-muscovite matrix. (f) Sample R228, staurolite porphyroblast with chlorite altered rim in quartz-muscovite matrix. Crystal controlled distribution of inclusions within porphyroblast core. Plane polarised light.



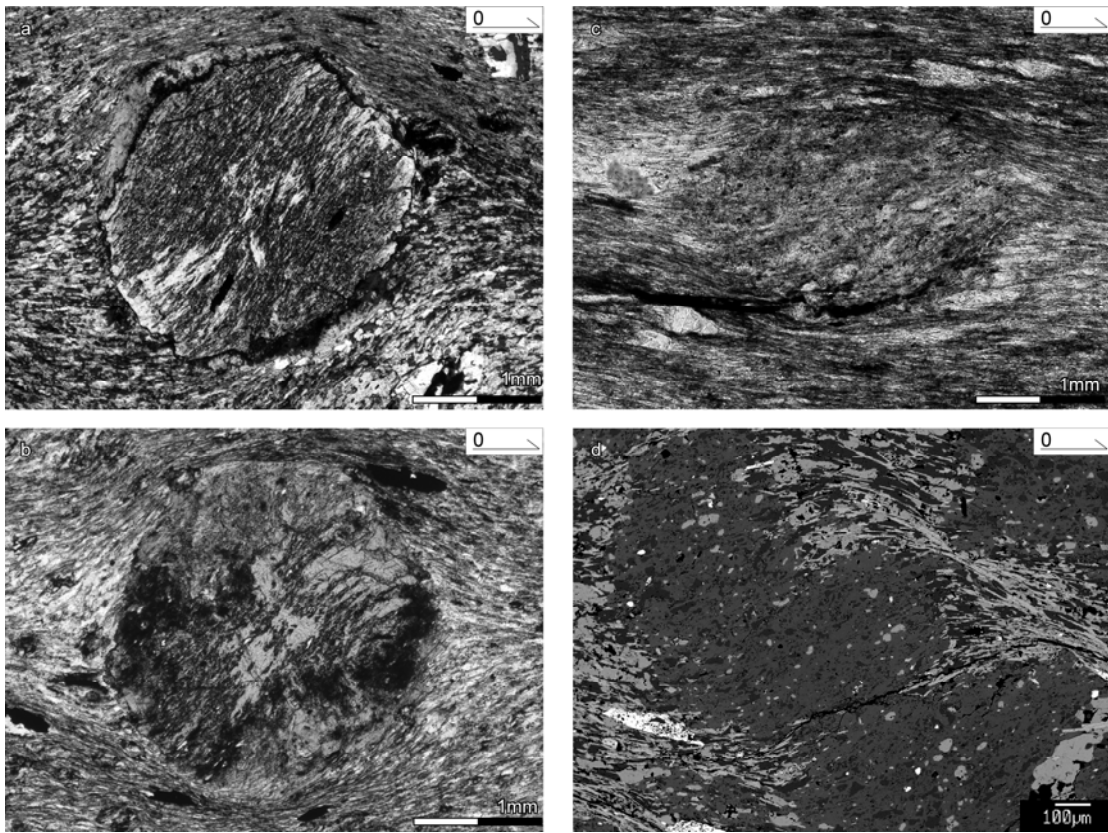


Figure 6. Photomicrographs from vertical thin sections orientated N (approximately perpendicular to the trend of FIA set 2). All porphyroblasts display inclusion trails with clockwise asymmetries. (a) Sample R244, garnet porphyroblast with chlorite alteration of quartz-muscovite matrix adjacent to rim. Plane polarised light. (b) Sample R241, chlorite altered garnet porphyroblast with quartz-muscovite matrix. Plane polarised light. (c) Sample R212, plagioclase porphyroblast in muscovite dominated matrix. Plane polarised light. (d) Sample R200, plagioclase porphyroblasts with muscovite-quartz matrix with aligned ilmenite lathes. Back scattered electron image.

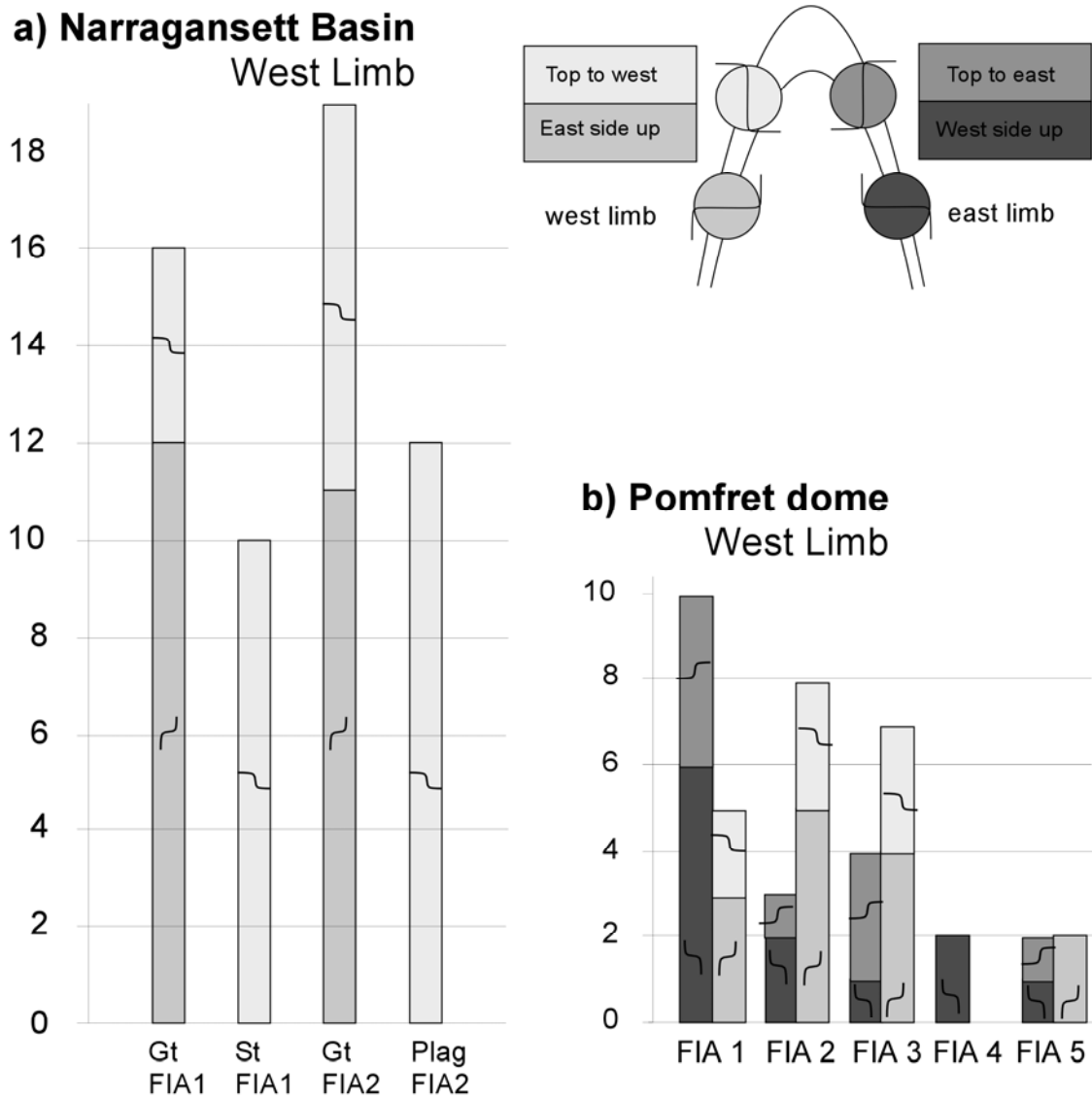


Figure 7. (a) Histogram showing the inclusion trail asymmetries for the two Rhode Island FIA trends recorded herein separated according to porphyroblast species. Shows all the asymmetries recorded were anticlockwise when determined for NW-SE section looking NE. (b) For comparison, the variable inclusion trail asymmetries for a single limb of the Pomfret Dome antiform (Bell et al., 2003).

Reference

Bell, T. H., Ham, A. P., Hickey, K. A. 2003. Early formed regional antiforms and synforms that fold younger matrix schistosity: their effect on sites of mineral growth. *Tectonophysics* 367, 253-278.

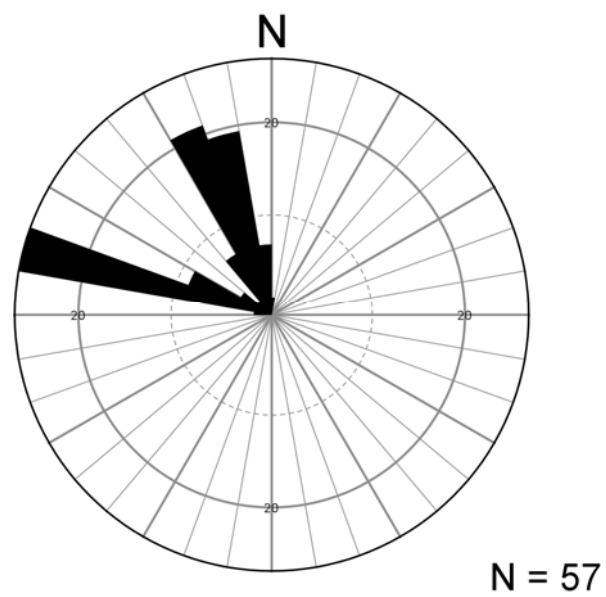


Figure 8. Wind vane diagram showing the direction of rotational shear along foliations preserved by porphyroblasts. WNW and NNW directed shear perpendicular to FIA set 1 and FIA set 2 respectively.

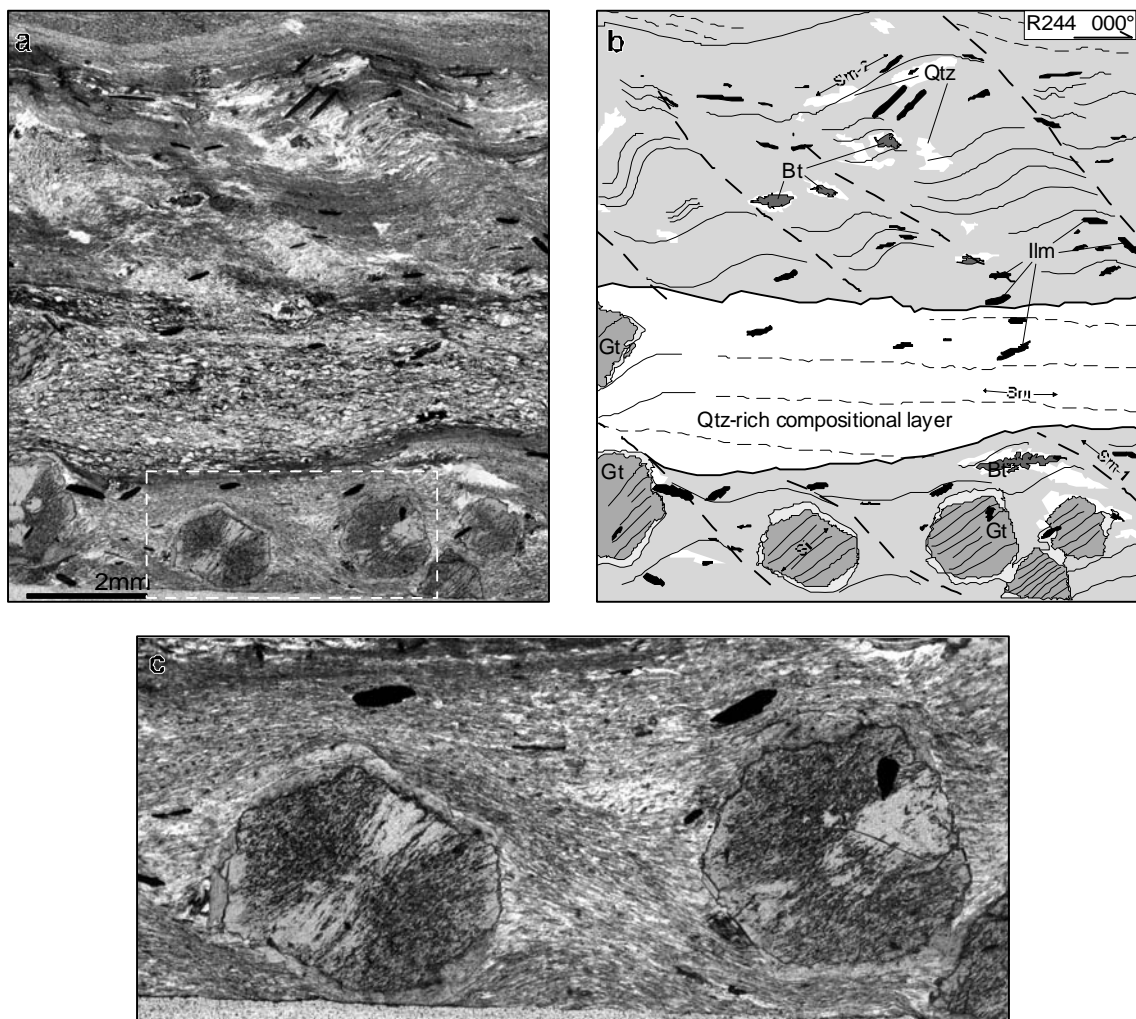


Figure 9. (a) Composite photomicrograph of sample R244. Single barbed arrow indicates way up and strike of vertical thin section. Photomicrographs taken in plane

polarised light. Dashed box shows location of inset (c). (b) Accompanying line diagram of (a), highlighting crenulation cleavage in the matrix, (S_{m-2}), which preserves the same asymmetry into differentiated crenulation cleavage seams, (S_{m-1}), as inclusion trails, (S_i), that are continuous with the external foliation, (S_m). (c) Enlarged view garnet porphyroblasts with continuous asymmetric inclusion trails.

Figure 10. (a) Cross-section from the south central zone of the Narragansett Basin as marked on figure 2. Pnb- Pennsylvanian Rhode Island Formation, Png- Permian Narragansett Pier Granite, Zav- Proterozoic Avalon crystalline basement. The approximate location of Conanicut Island is marked by the box labelled d'. (b) to (c) are diagrammatic representations of stages during the formation of the overturned fold at d'. An inset from each limb at the position marked by a circle is presented on either side of the fold. (b) An upright F_1 fold. Differentiated crenulation cleavage has opposite asymmetry on either side of the fold. (c) Non-coaxial W directed compression producing a westward sense of shear from the vertical foliation into the horizontal crenulated cleavage on the west fold limb. On the east fold limb, bedding is reactivated and the weakly formed crenulation is decrenulated. (d) Continued non-coaxial deformation and bulk westward displacement overturns the west fold limb and S_0 reactivates. Continued reactivation of bedding on the east fold limb creates a pervasive bedding parallel foliation.

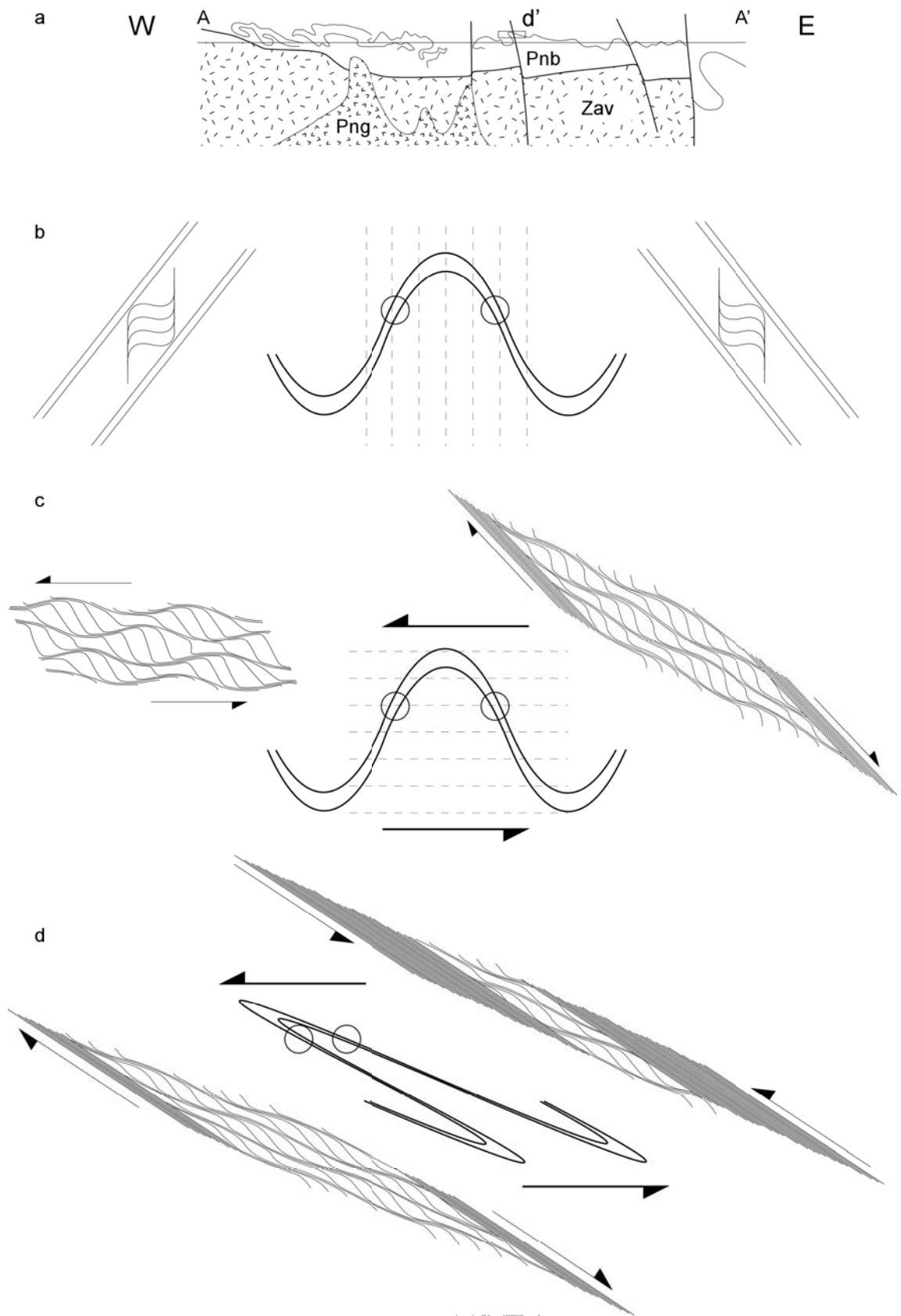
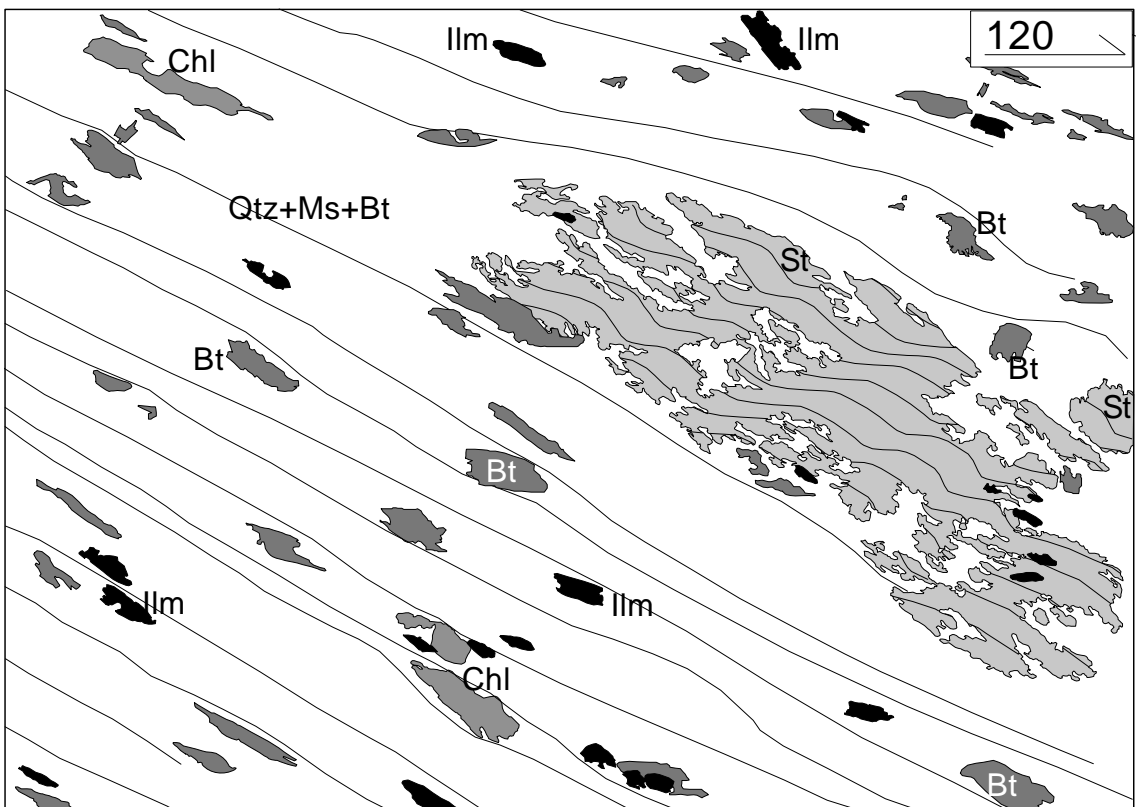
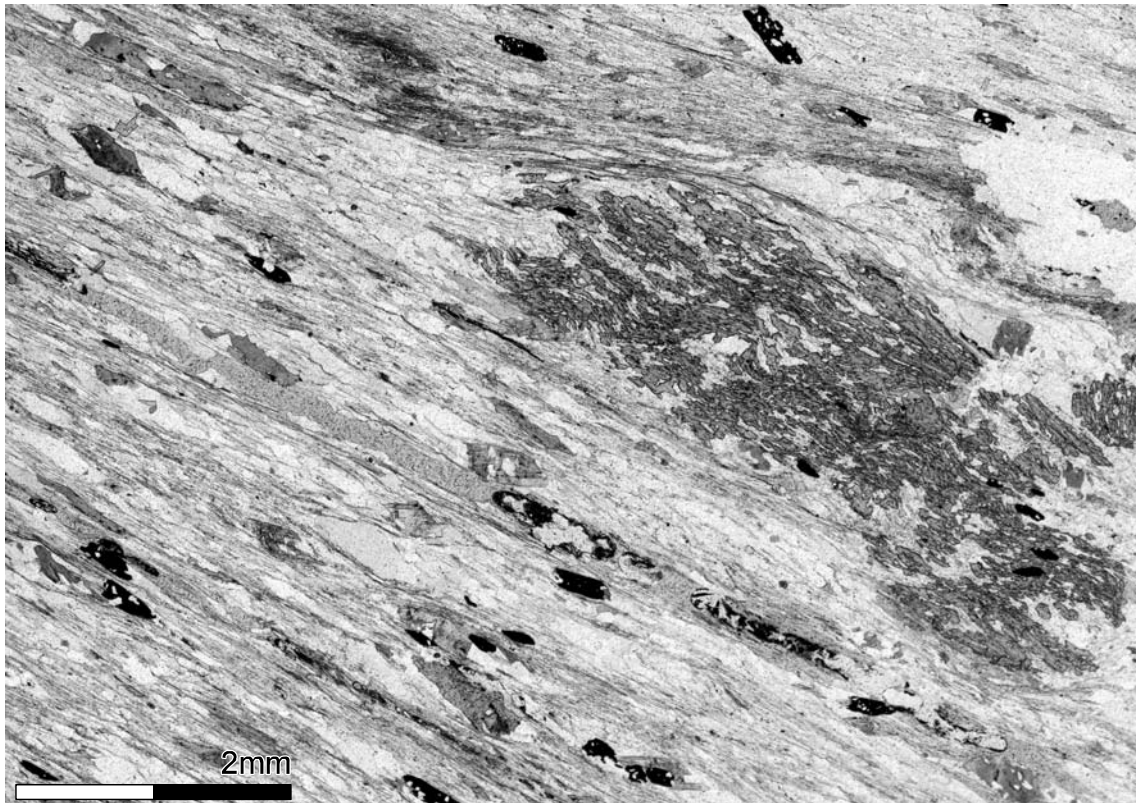


Figure 11. Photomicrograph and accompanying line diagram from vertical thin sections of sample R125 orientated at N120°E. Shows a staurolite porphyroblast that has overgrown a differentiated crenulation cleavage. Reactivation of the foliation during progressive shearing has decrenulated the pre-existing crenulations within the matrix. Plane polarised light.



**Chapter 3. Progressive changes in bulk movement
direction and shear sense during the transition from
Acadian to Alleghanian orogenesis.**

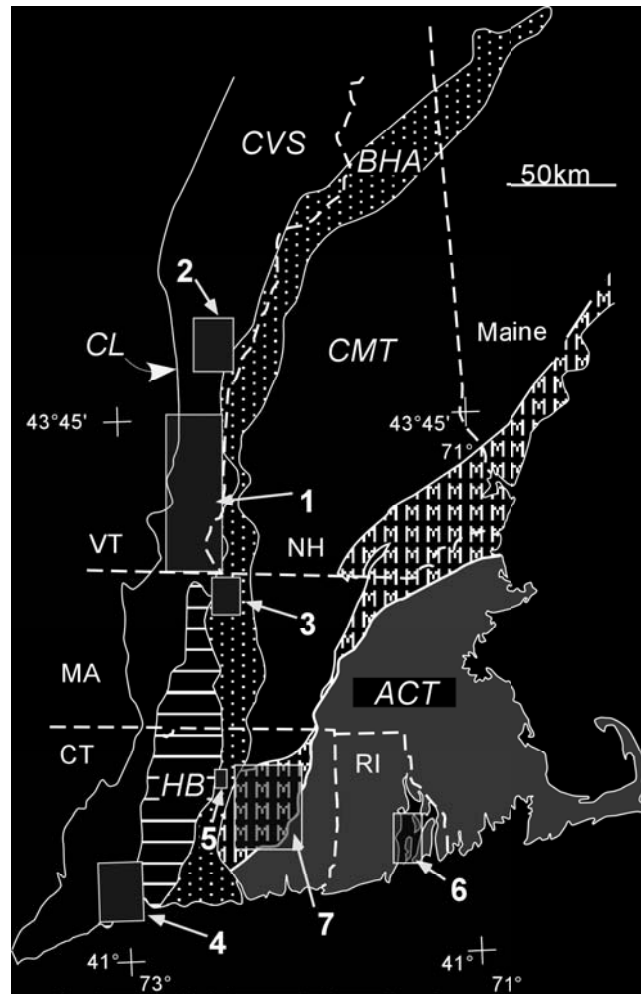


Figure 1. Regional tectonic map, with state borders, of the New England Appalachian Orogenic Belt illustrating the main lithotectonic terranes discussed in the text. *CVS* - Connecticut Valley Synclinorium, *HB* - Hartford Basin, *BHA* - Bronson Hill Anticlinorium, *CMT* - Central Maine Terrane, *ACT* - Avalon Composite Terrane. The Merrimack Terrane has been ornamented with the letter M. Cameron's Line (*CL*) is a tectonic boundary separating Taconic metamorphism in the west from Acadian metamorphism in the east. Boxes represent the approximate extent of field areas referred to in the text; 1) southeast Vermont, 2) east central Vermont, 3) north central Massachusetts, 4) south central Connecticut, 5) north central Connecticut (the Bolton Syncline), 6) Narragansett Basin and 7) eastern Connecticut (the Merrimack Terrane; Fig. 2).

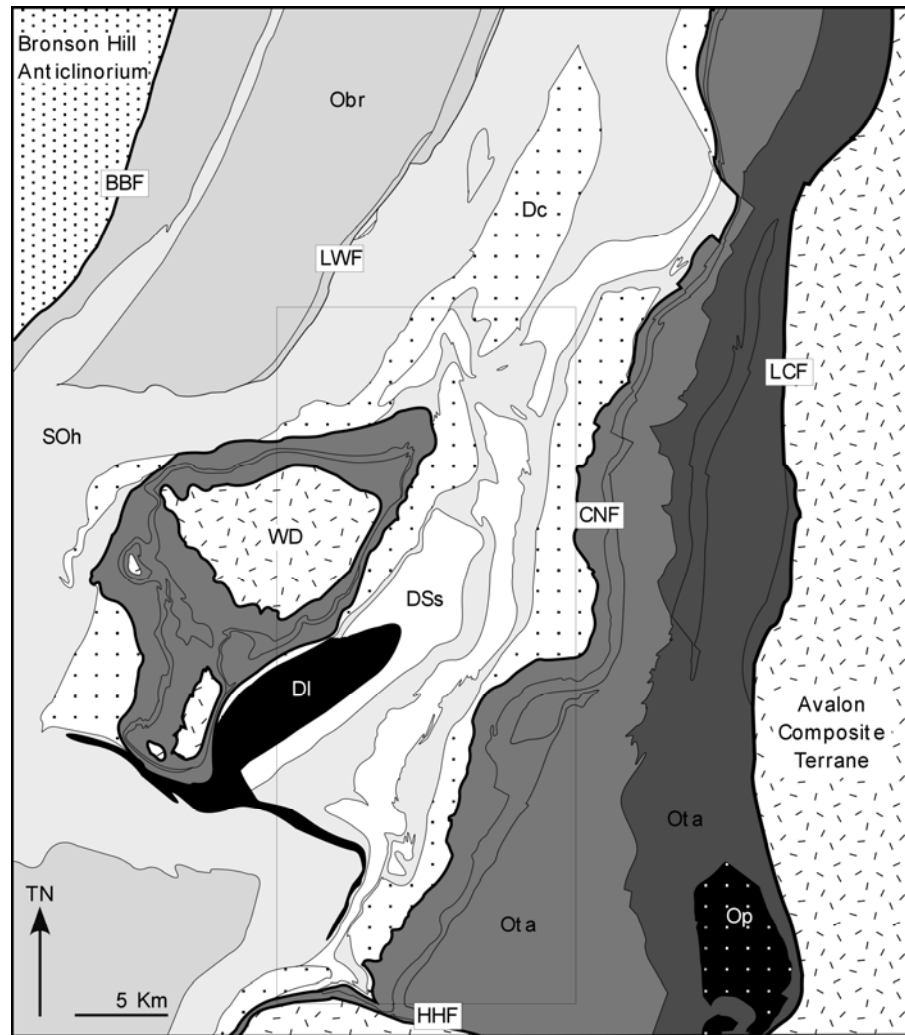


Figure 2. Lithological map of a part of eastern Connecticut modified from Rodgers (1985). Major terrane bounding faults are labelled; BBF – Bonemill Brook, LWF – Lake Wangumaug, CNF – Clinton Newbury, LCF – Lake Char, HHF – Honey Hill. Geologic formations are labelled; Obr – Ordovician Brimfield Schist, Dc – Devonian Canterbury Gneiss, SOh – Silurian-Ordovician Hebron Gneiss, DI – Devonian Lebanon Gabbro, Ota, Ordovician Tatnic Hill Formation, Op – Ordovician Preston Gabbro and DSS – Devonian-Silurian Scotland Schist. The Willimantic Dome is labelled WD. The location of the area shown in Figure 3 is outlined with a box.

Reference

Rodgers, J. 1985. Bedrock geological map of Connecticut. U. S. Geological Survey, Connecticut Geological and natural History Survey.

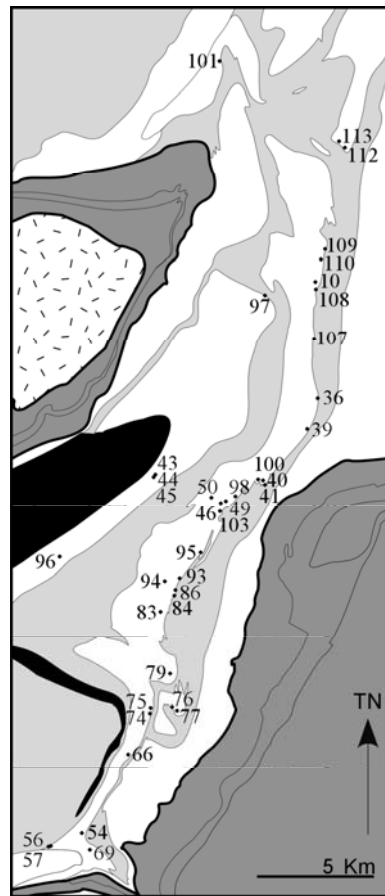
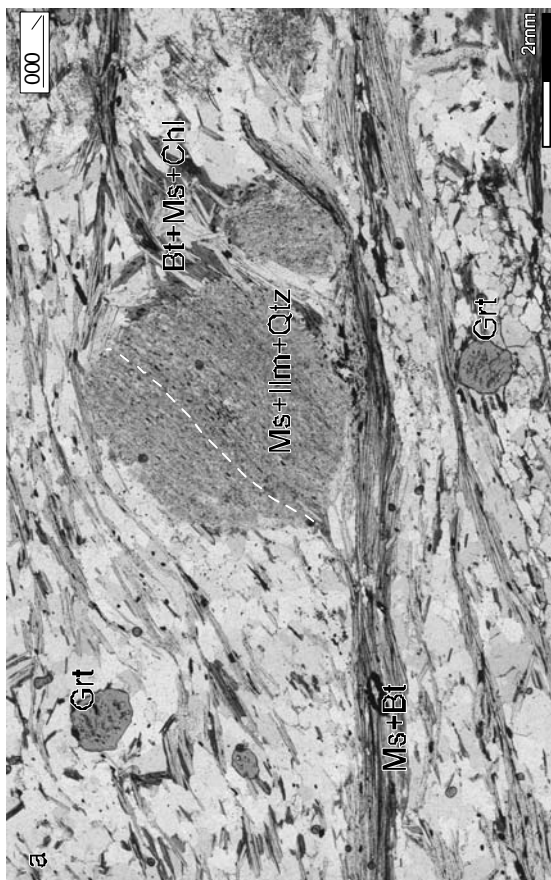
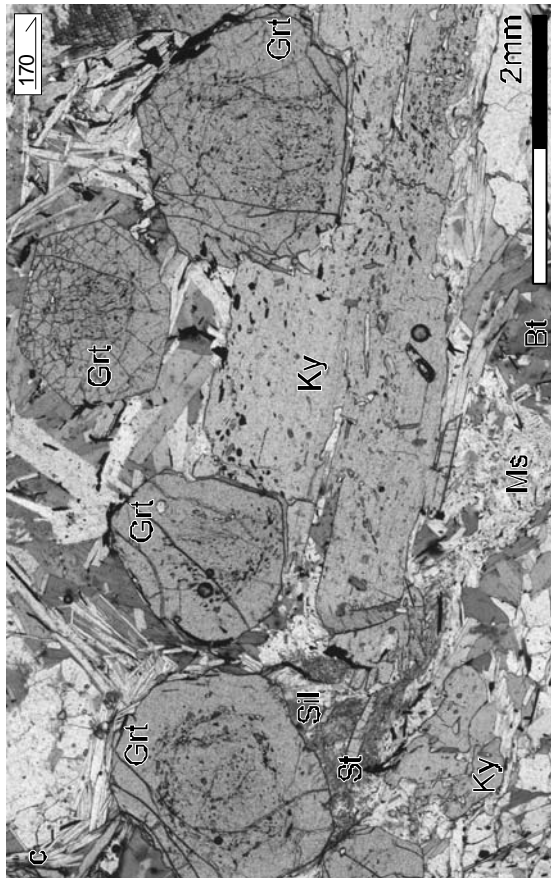


Figure 3. Geologic map showing the location of samples used for microstructural analysis within the Merrimack Terrane of eastern Connecticut. Samples were collected from the Devonian-Silurian Scotland Schist.

Table 1. Garnet and staurolite FIA trends measured from samples collected from the Scotland Schist. Garnet multi-FIA sample FIAs are referred to as either ‘Core FIA’, ‘Median FIA’, or ‘Rim FIA’ based on their relative location inside the porphyroblasts. Single-FIA samples are presented in the ‘Core FIA’ column. Trends are presented relative to true north. The major mineral phases are recorded for each sample.

Figure 4. Photomicrographs of samples from the Scotland Schist. Single barbed arrow indicates up direction and strike of vertical thin sections. Photomicrographs taken in plane polarised light. a) Sample R10, staurolite pseudomorphs of muscovite, ilmenite and quartz with relict sigmoidal inclusion trails defined by ilmenite. Garnet porphyroblasts have the same inclusion trail asymmetry as staurolite pseudomorph. The matrix within quartz dominated zones has a well defined clockwise asymmetry on the foliation into the horizontal differentiated crenulation. b) Sample R35, kyanite grains and fibrolitic sillimanite aligned with the matrix foliation defined by elongate quartz, muscovite and biotite. c) Sample R96, garnet porphyroblasts with anticlockwise inclusion trails in their cores. A large kyanite porphyroblast has overgrown a foliation that is continuous with an included foliation in the rims of the garnet porphyroblasts. Fibrolitic sillimanite has grown in the strain shadow of the garnet and kyanite porphyroblasts. A small, late forming tabular grain of staurolite has grown within the fibrolite. d) Sample R51, the pervasive matrix foliation defined by muscovite, biotite and ilmenite has been crenulated. Inclusion trails in staurolite have varying degrees on continuity with the matrix foliation. Chlorite has overgrown the crenulated foliation.



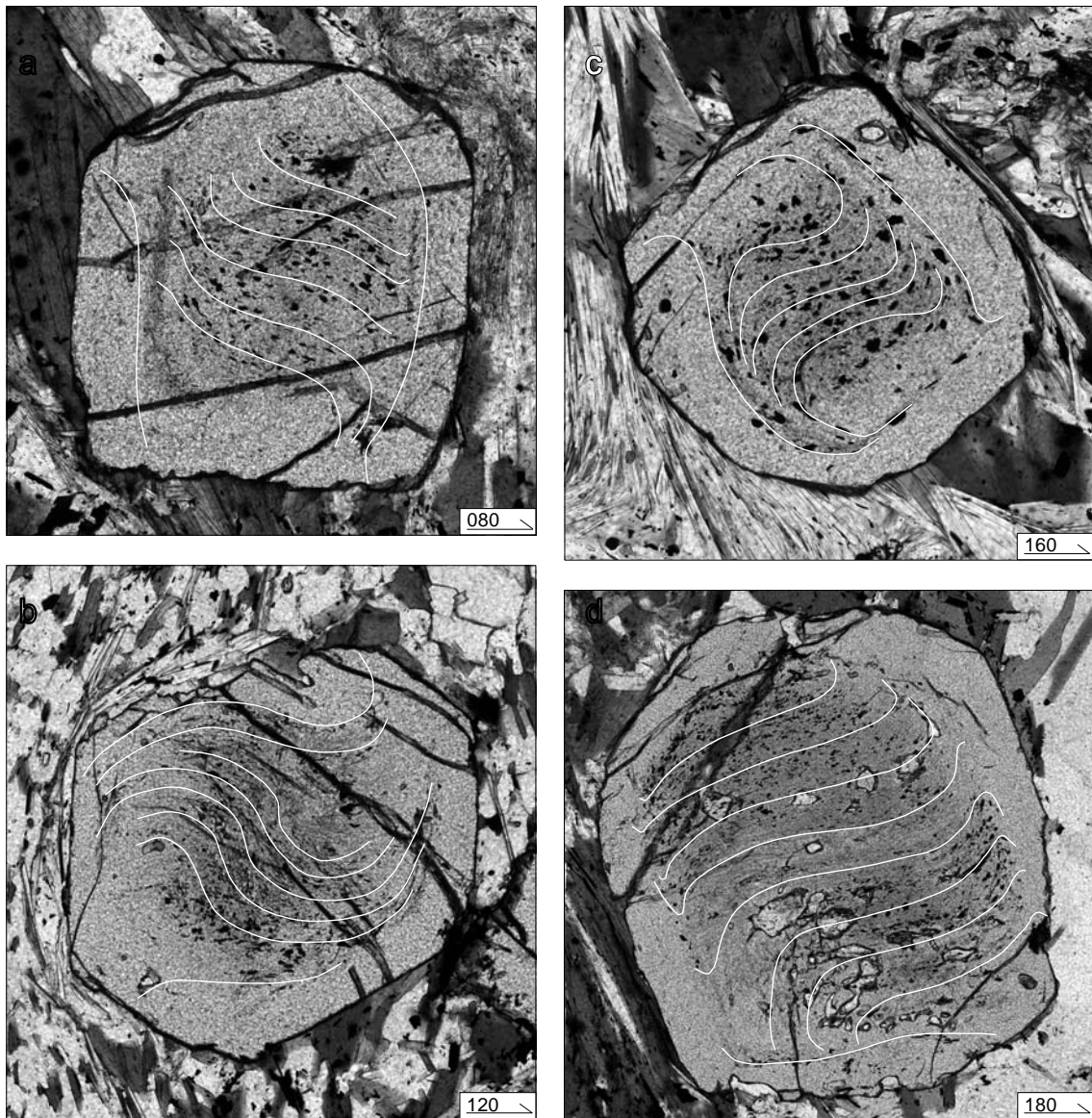
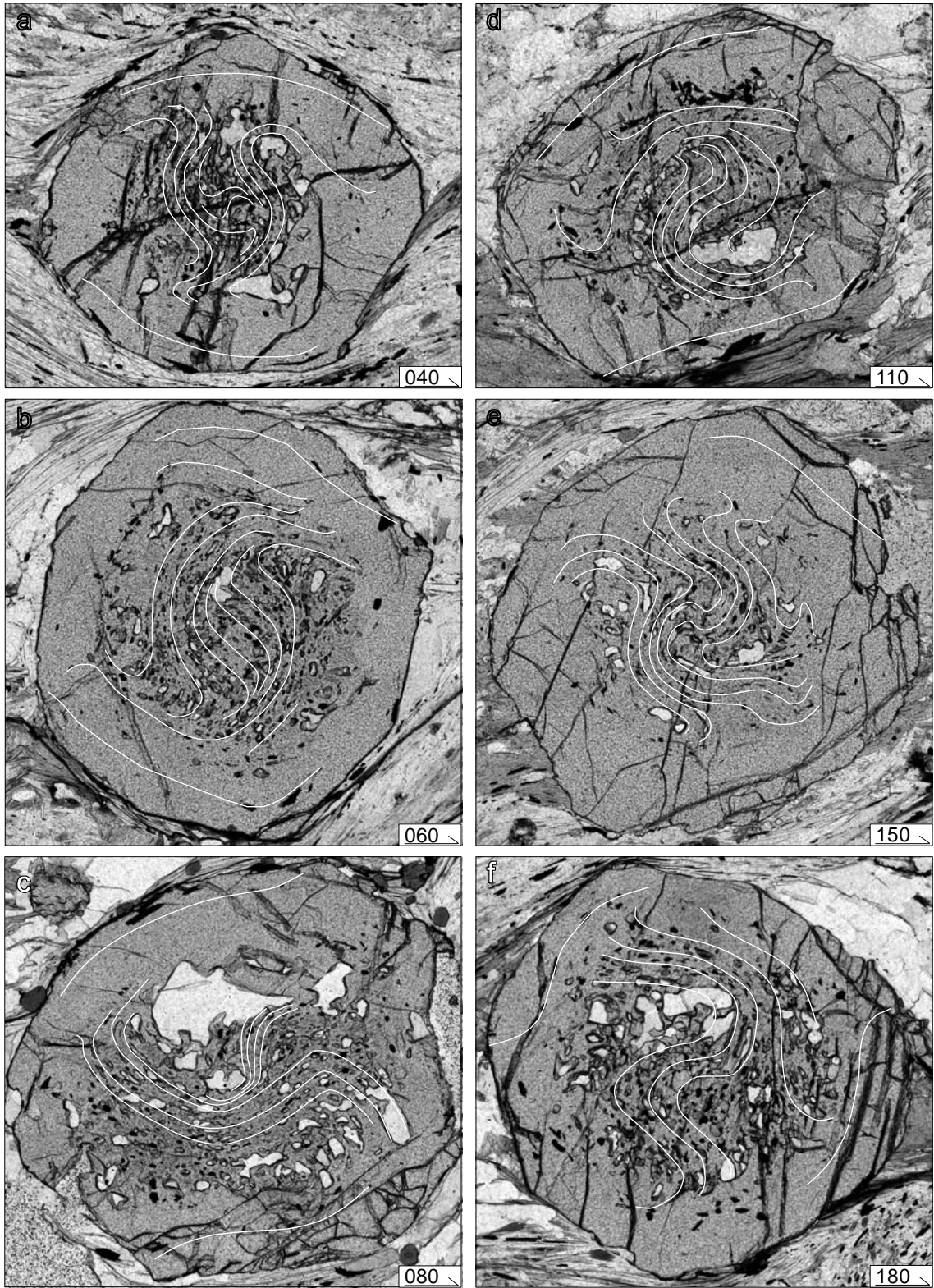


Figure 5. Photomicrographs taken in plane polarised light of garnet porphyroblasts from sample R96. Single barbed arrow indicates up direction and strike of vertical thin sections. The sigmoidal inclusion trails in the cores of the porphyroblasts flip asymmetry between the sections striking at 80° and 120° . A flip in the asymmetry of the rim inclusion trails occurs between the sections striking at 160° and 180° . Phases of garnet growth are distinguishable using changes in inclusion density, mineral species or geometry from one part of the porphyroblast to another. This sample has inclusion-rich cores but inclusion-poor rims. Photomicrographs taken in plane polarised light.

Figure 6. Photomicrographs taken in plane polarised light of garnet porphyroblasts from sample R66. Single barbed arrow indicates up direction and strike of vertical thin sections. The sigmoidal inclusion trails in the cores of the porphyroblasts flip asymmetry between the sections striking at 080 and 110. The inclusion trails in the median of the porphyroblasts are flipping asymmetry close to the section striking at 040. A flip in the asymmetry of the rim inclusion trails occurs between the sections striking at 150 and 180. By utilising established concepts of overprinting criteria, analysis of a multi-FIA sample can allow a succession of FIAs to be determined in the one sample. Data from all samples can then be combined and if a consistent relative succession results, the relative timing of each FIA can be derived (Bell et al., 2003).



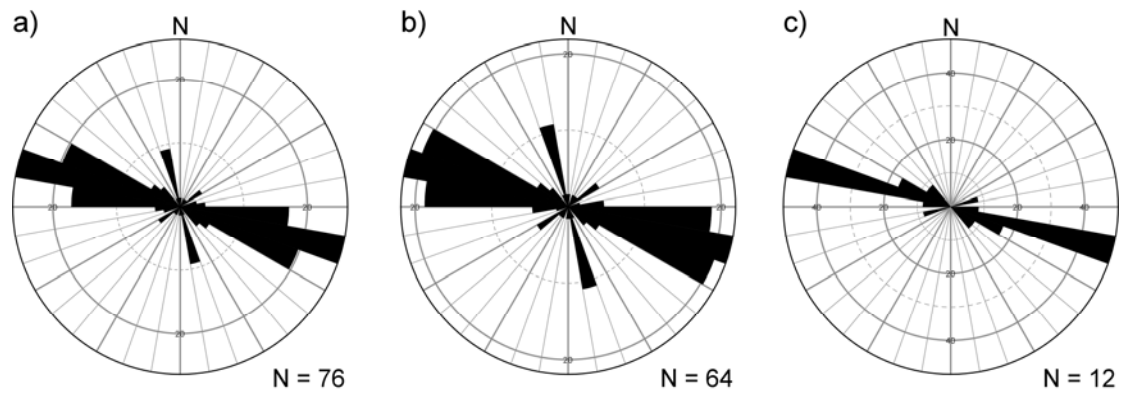


Figure 7. Equal area Rose plots of FIA trends measured for garnet and staurolite porphyroblasts from the Scotland Schist of the Merrimack Terrane. (a) All FIA. (b) Garnet samples. (c) Staurolite samples. Three clusters of FIA trends are visible oriented WNW-ESE, NNW-SSE and SW-NE.

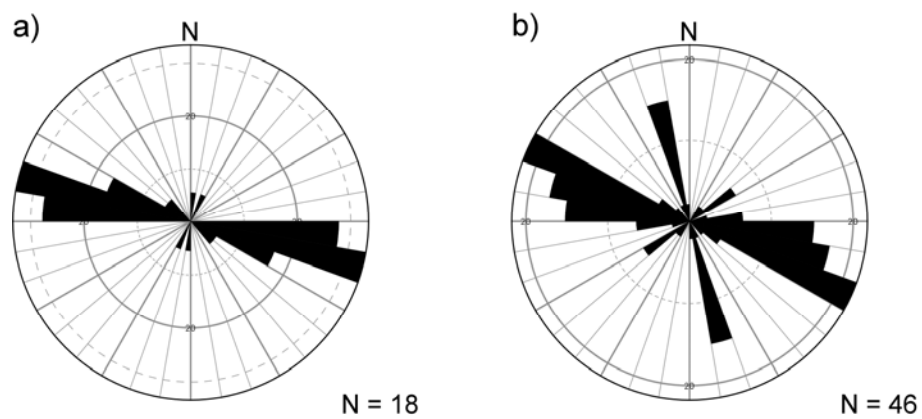


Figure 8. Equal area Rose plots of FIA trends separated as (a) single-axis or (b) multi-axis samples. One principal trend oriented WNW-ESE is visible in the single FIA plot. The multiple FIA data shows three clusters of trends, oriented WNW-ESE, NNW-SSE and SW-NE.

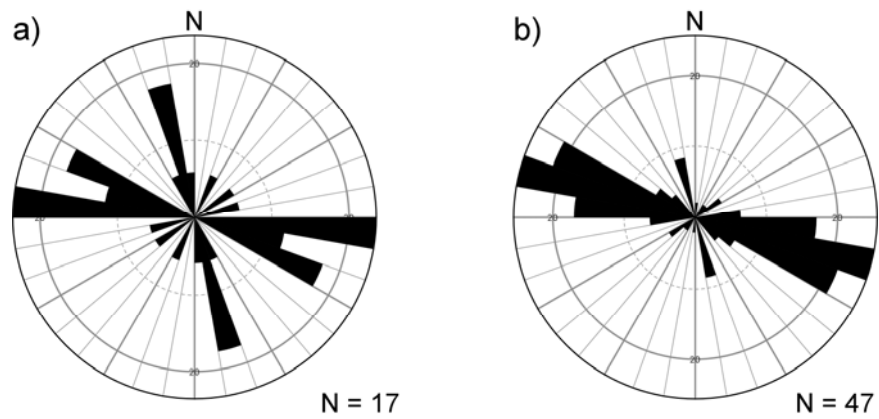


Figure 9. Equal area Rose plots of FIA trends separated according to whether the inclusion trails are dominantly (a) continuous or (b) truncated by the matrix foliation. 9a shows trends oriented WNW-ESE and NNW-SSE. 9b displays a dominant trend oriented at WNW-ESE and small clusters oriented NNW-SSE and SW-NE.

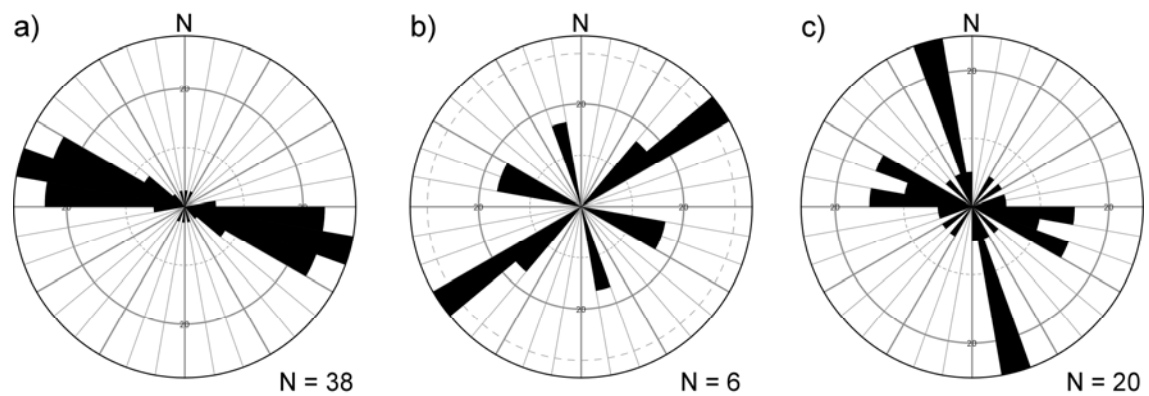


Figure 10. Equal area Rose plots of FIA trends separated as (a) core, (b) median and (c) rim trends. 9a shows a single dominant trend oriented WNW-ESE. 9b shows three peaks oriented SW-NE, NNW-SSE and WNW-ESE. 9c shows two dominant peaks oriented NNW-SSE and WNW-ESE.

Table 2. Test of the null hypothesis, H_0 , that the FIAs measured in rocks from eastern Connecticut are a sample of a random population using Watson's U^2 test statistic for grouped data. The result greatly exceeds the U^2 value at the 0.01 level of significance, suggesting the null hypothesis, H_0 , can be rejected and that the population is not random. (FIA trends were initially doubled to convert them from axial data to directional data; modulo 360° .)

Table 2

j	n _j	S _j	(S _j) ²
360°-009°	1	-1.056	1.114
010°-019°	0	-3.111	9.679
020°	0	-5.167	26.694
030°	0	-7.222	52.160
040°	1	-8.278	68.522
050°	0	-10.333	106.778
060°	1	-11.389	129.707
070°	0	-13.444	180.753
080°	0	-15.500	240.250
090°	0	-17.556	308.198
100°	3	-16.611	275.929
110°	0	-18.667	348.444
120°	0	-20.722	429.410
130°	0	-22.778	518.827
140°	2	-22.833	521.361
150°	0	-24.889	619.457
160°	3	-23.944	573.336
170°	0	-26.000	676.000
180°	13	-15.056	226.670
190°	0	-17.111	292.790
200°	19	-0.167	0.028
210°	0	-2.222	4.938
220°	15	10.722	114.966
230°	0	8.667	75.111
240°	4	10.611	112.596
250°	0	8.556	73.198
260°	3	9.500	90.250
270°	0	7.444	55.420
280°	0	5.389	29.040
290°	0	3.333	11.111
300°	1	2.278	5.188
310°	0	0.222	0.049
320°	7	5.167	26.694
330°	0	3.111	9.679
340°	1	2.056	4.225
350°-359°	0	0.000	0.000
TOTAL	74	-227.000	6218.574

$S_j = \text{sum of } (n_j - np_j)$.

$U^2_G = 1/nk \{ S^2_T - 1/k(S_j)^2 \}$.

$U^2_G = 1.797$.

highly significant at $p=0.01$ ($U^2_G=0.268$).

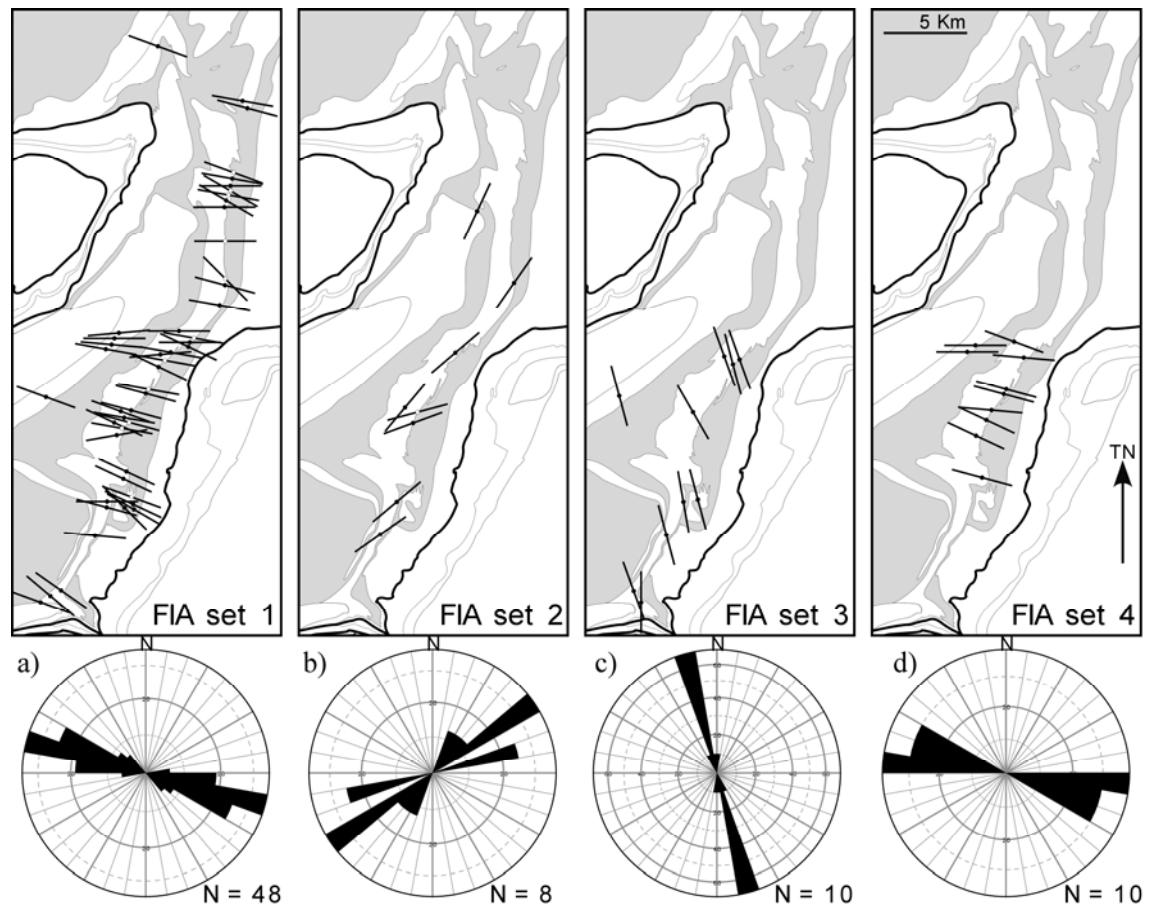


Figure 11. FIA trends for successive FIA sets in the Scotland Schist of the Merrimack Terrane. (a) Map of FIA set 1 trends. (b) Map of FIA set 2 trends. (c) Map of FIA set 3 trends. (d) Map of FIA set 4 trends.



Figure 12. Map showing the distribution of dominant ACW versus CW differentiation asymmetry in the matrix. The majority of samples record an anticlockwise differentiation asymmetry (black arrow) looking NE for curvature of a sub-vertical crenulated cleavage into a sub-horizontal differentiated crenulation cleavage seam. The location of the area is shown in Figure 2.

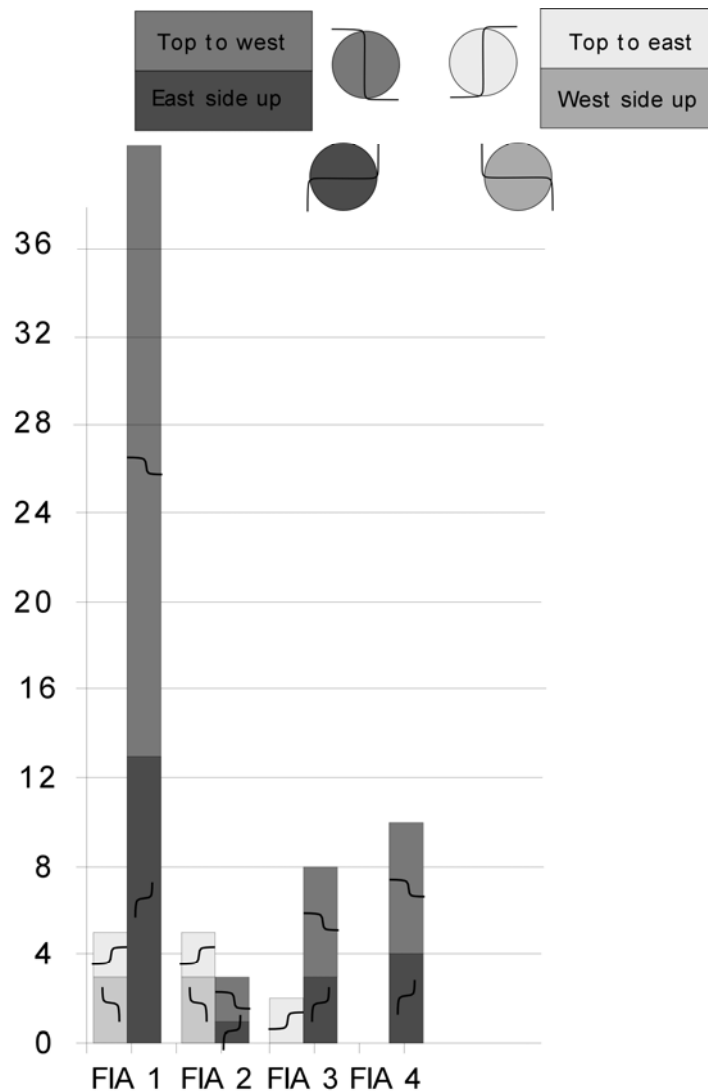


Figure 13. A histogram showing the asymmetry of inclusion trails preserved within porphyroblasts from the Scotland Schist. They have been separated according to FIA sets. Also indicated is whether the inclusion trail geometry can be interpreted as resulting from a flat to steep transition or a steep-to-flat transition of successive foliations. The asymmetries defining WNW-ESE trending FIAs, sets 1 and 4, were determined from vertical thin sections near orthogonal to this trend looking WNW. Those for sets 2 and 3 were determined looking NE and NNW, respectively.

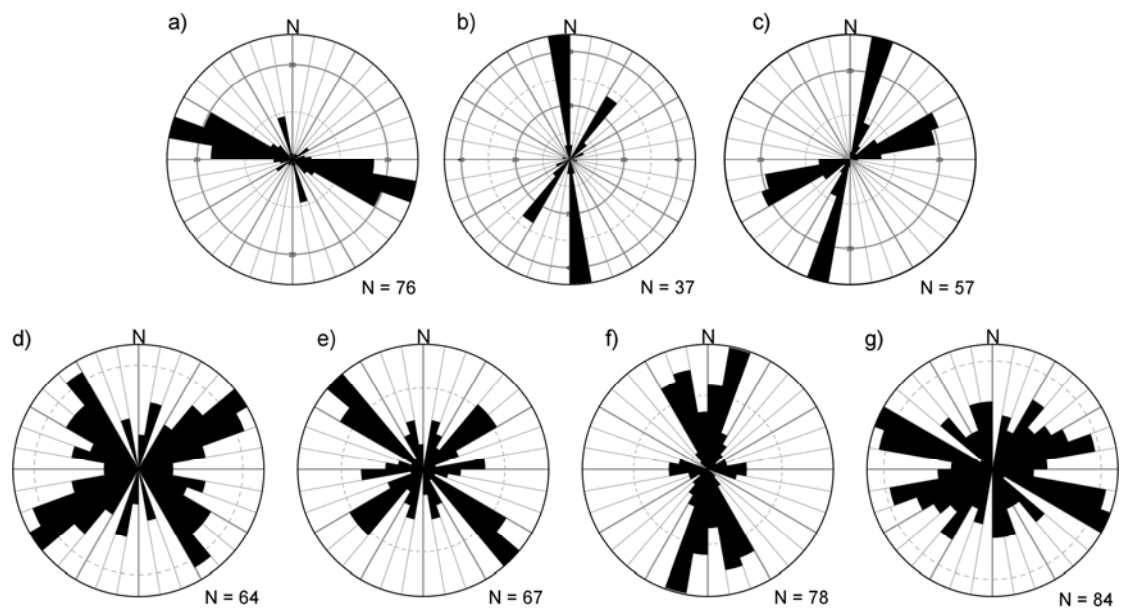


Figure 14. Equal area Rose plots of FIA trends measured from the (a) Scotland Schist, (b) Bolton Syncline, north central Connecticut, (c) Narragansett Basin, Rhode Island, (d) north central Massachusetts, (e) east central Vermont, (f) south east Vermont and (g) south central Connecticut.